ANNALS OF GEOPHYSICS, 67, 3, S325, 2024; doi:10.4401/ag-9116
OPEN ACCESS

# Predict: Assessing the Seismic Response in the city of Rome, Part 1. New Data for a Geologic Overview

Fabrizio Marra[*,1], Carlo Rosa[2], Daniele Silvestri[1,3], Paola Bordoni[1], Francesca Bulian[4], Fabio Florindo[1], Brian R. Jicha[5], Fabrizio Cara[1], Daniela Famiani[1], Riccardo Salvini[3]

(1) Istituto Nazionale di Geofisica e Vulcanologia, Roma, Italy
(2) SIGEA Lazio – APS, Roma, Italy
(3) University of Siena, Department of Physical Sciences, Earth and Environment, Siena, Italy
(4) University of Groningen, Institute of Archaeology, Groningen, The Netherlands
(5) University of Wisconsin-Madison, Department of Geoscience, Madison, USA

Article history: received May 28, 2024; accepted July 19, 2024

## Abstract

This work presents the preliminary results of the stratigraphic, paleomagnetic, micropaleontologic and geochronologic investigations carried out on the cores of three boreholes performed in the historic center of Rome within the Predict Project, aimed at evaluating the seismic response within the City through the 3D modeling of the subsoil.
Moreover, we have integrated the investigations on the cores of four previously performed boreholes and we use this larger dataset to provide an objective element for the interpretation and validation of a large databank of paper stratigraphies of boreholes carried out for civil engineering purposes in the Roman area.
The new data are presented within an exhaustive review of state of the art on the scientific knowledge on the geology of Rome, aimed at providing an updated background for the Quaternary scientists, seismologists, engineers and professional technicians operating in this region.
Within this framework, we provide a detailed reconstruction of the chronostratigraphic setting in central Rome, highlighting a coherent picture within the glacio-eustatic control on the sedimentary processes and providing the background geological input data for the creation of a geo-database in a dynamic GIS environment, which is the subject of a forthcoming sister-paper.

Keywords: Geology of Rome; Quaternary stratigraphy; $^{40}Ar/^{39}Ar$ Geochronology; Paleomagnetism; Micropaleontology

## 1. Introduction

A new methodology was developed for the multidimensional and multi-scale analysis of the geological substrate of the historic center of the city of Rome, aimed at 3D geological modeling of the subsoil, as part of the ST-Predict Project in the framework of the of Dynamic Planet – Working Earth project (https://progetti.ingv.it/it/pian-din). The ultimate goal of 3D geological modeling is to identify and evaluate the volumes of lithological units, which will

be associated with geophysical and geotechnical units and transformed into a numerical model for seismic wave propagation simulations dedicated to predicting surface shaking.

For this purpose, the execution of three boreholes was planned in key areas of the historic center, aimed at providing original data on the mechanical characteristics of the soil, through the execution of borehole geophysical measures. Moreover, the direct observations on the geological-stratigraphic characteristics of the main sedimentary and volcanic terrains provide a means to validate the interpretation of the numerous borehole stratigraphies used for the reconstruction of the geological substrate.

A fundamental tool for the geological modeling of Rome is in fact the large quantity of drilling data available, which represents a significant contribution in subsurface observations. In particular, a databank of several thousand geognostic surveys was created over the years by the Istituto Nazionale di Geofisica e Vulcanologia (INGV) as part of various degree theses through the collection of paper stratigraphies of boreholes carried out for civil engineering purposes in the Roman area. This databank was also integrated by several core surveys carried out for scientific study purposes as part of dedicated research projects, financed by INGV. Such direct observations make it possible to implement the geological knowledge acquired through outcrop data and, above all, they provide an objective element for the interpretation and validation of the paper stratigraphies contained in the databank, generally carried out by personnel who were not experts in the stratigraphy of Rome, and dedicated to geotechnical purposes, other than strictly geological-stratigraphic ones.

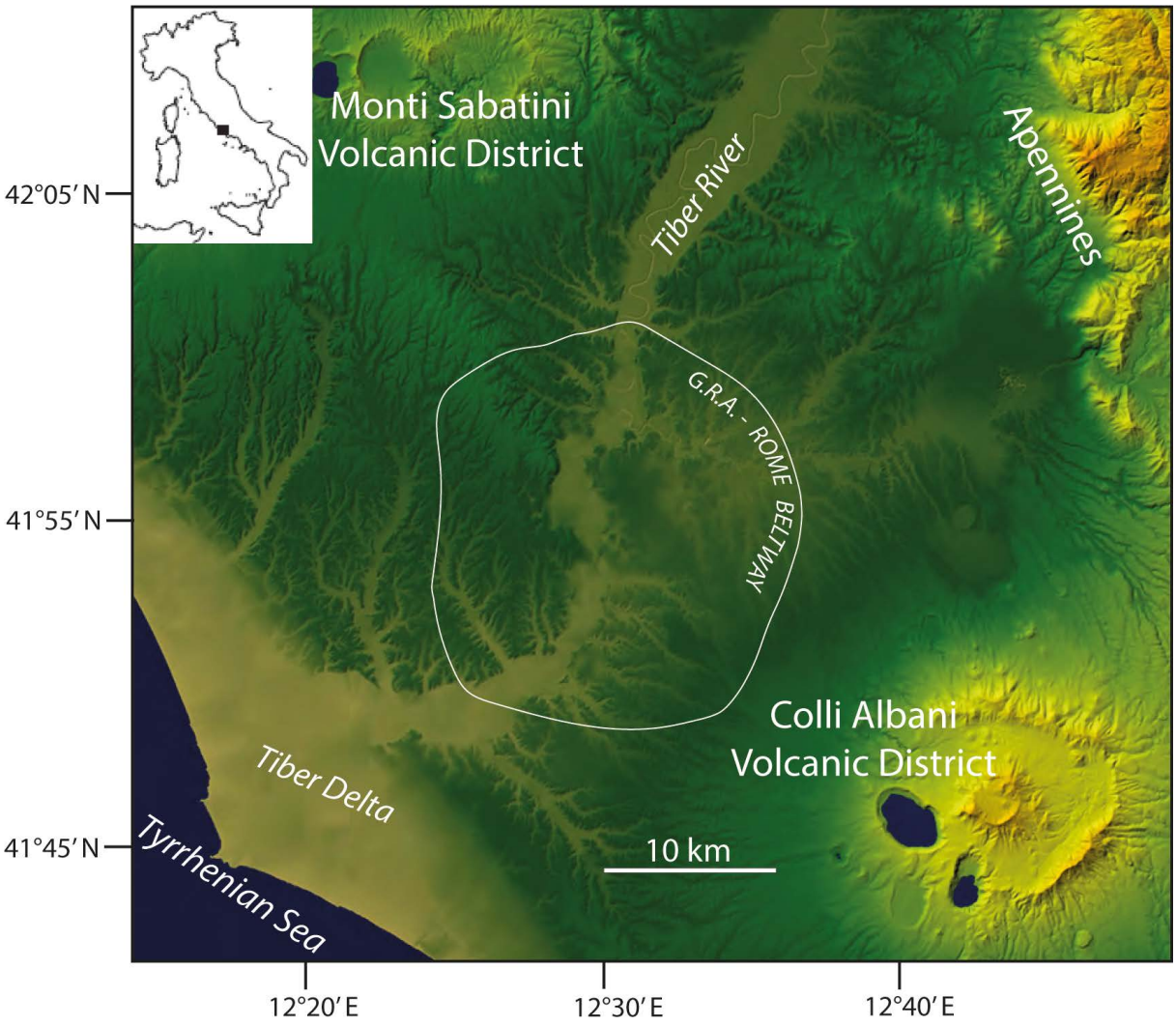


**Figure 1.** DEM image of the area of Rome. This region has served as a natural laboratory for the study of the climatic cyclicality of the Pleistocene thanks to a series of concomitant factors: it is close to the coast, it is crossed by a large river that drains the slopes of the Apennine chain, and it is between two large volcanic districts which have been active for the last 800,000 years, providing the material that allows dating of the sedimentary successions.

This work describes the preliminary results of the three boreholes performed and their framing in the stratigraphic context of the historic center of Rome, with the aim of integrating current knowledge on the geology of this area and providing a detailed framework of geological input data for the creation of a geo-database (GDB) in a dynamic GIS environment.

A sister paper [Silvestri et al., forthcoming] presents the results of the study aimed at creating this geo-database, the 3D model and the preliminary results of the geological modeling.

## 2. Geologic and Structural Setting

The sediments and rocks that constitute the substrate of the city of Rome were generated by the interaction between different geological processes, which in turn were determined by regional geodynamic and paleogeographic factors.

The Roman area is located on a continental margin (the Tyrrhenian Sea margin) representing a back-arc geodynamic domain, originated by the subduction of the Adrian microplate and the northeastern migration of the slab [Malinverno and Ryan, 1986]. The extensional tectonic regime acting in this region since Tortonian times [Patacca et al., 1990] generated the Tyrrhenian marine basins and facilitated the uprising of magma originated by the fusion of the subducted slab [Serri et al., 1993], which ultimately gave birth to the volcanic districts of the "Roman Magmatic Province" during the Middle Pleistocene [Peccerillo, 2017].

From the Pliocene to the Early Pleistocene, the Roman area was characterized by marine conditions. In this period of time the clayey sediments which constitute the oldest terrains outcropping today within the City are deposited: the Monte Vaticano Unit [Marra et al., 1995, and ref. therein; Lower Pliocene] and, after a temporary phase of emergence, the Farneto Silts [Marra, 1993; Bergamin et al., 2002; Cosentino et al., 2008; Lower Pleistocene]. The latter continuously pass to sands of a coastal environment ["*Sabbie ad Artica islandica*", Bonadonna, 1968; Cosentino et al., 2008] which mark the beginning of a regressive phase that leads to the definitive continentalization of part of the Roman area, with a coastline that crossed the center of the city diagonally from south-west to north-east.

The rise of magma in the crust is the cause of the progressive uplifting, which leads to the formation of a paleo-delta of the Tiber starting from ca. 1.3 Ma [Florindo et al., 2024, and ref. therein], coinciding with the beginning of the first highly potassic volcanic activity in the Cimini Mountains [Barberi et al., 1994; Peccerillo, 2017].

From this point on, sedimentary processes in the Rome area are restricted to river channels and the coastal plain and are strictly controlled by the interplay between sea level changes related to glacio-eustatism, volcanic activity and tectonics [Marra and Rosa, 1995; Karner and Marra, 1998; Luberti et al., 2017]. In the interval 1.3-0.8 Ma, characterized by scanty volcanic activity, a series of "aggradational successions" [Marra et al., 2016a, Giaccio et al., 2021] were deposited in the Rome area in response to the sea-level oscillations corresponding to the marine isotopic stages (MIS) 35-19 [Florindo et al., 2024]. These are alternations of gravels and clays that were deposited in the coastal plain and accumulated thanks to a slow and continuous subsidence within the "Paleotiber Graben": a tectonic depression trending from NW-SE to N-S, originating from extensional forces responsible for the rise of magmas and the birth of volcanic districts in the Middle Pleistocene [Marra and Rosa, 1995; Marra and Florindo, 2014].

Starting from 0.6 Ma, huge pyroclastic flow deposits, several tens of $km^3$ in volume, and subordinately fallout deposits and lava flows, are erupted from the Monti Sabatini and Colli Albani districts, located respectively NW and SE of Rome [Fornaseri et al., 1963; Mattias and Ventriglia, 1970; De Rita et al., 1988; Karner et al., 2001a; Giordano et al., 2006; Sottili et al., 2010; Marra et al., 2009, 2014, 2020; Gaeta et al., 2016]. These stratified volcanic deposits, represented by tuff, pozzolan and ash, constitute the geological substrate above the gravelly-clayey successions of the Paleotiber in the morphologically higher sectors, while they are intercalated with sedimentary deposits within the fluvial paleoincisions [Marra and Rosa, 1995; Funiciello et al., 2008].

Traditionally, the $\geq 600$ ka aggradational successions have been defined as the "pre-volcanic" Paleotiber successions, as opposed to the $< 600$ ka, sin-volcanic, Paleotiber successions. The latter are also equivalent to the "Fluvial-lacustrine" successions of the early literature [e.g., Ventriglia, 1971]. Four Paleotiber successions, correlating with MIS 21, MIS 19, MIS 18.3/19.3, and MIS 15 have been proposed based on available $^{40}Ar/^{39}Ar$ and paleomagnetic constraints in the subsurface of Rome: PT1, PT2, PT3, and PT4 [Marra and Florindo, 2014]. These correspond to the Monte Ciocci, Ponte Galeria 1, Ponte Galeria 2, and Santa Cecilia Formations [Marra et al., 1998]. However, an older age for the Monte Ciocci Formation, lacking direct geochronologic constraints, was hypothesized in Marra et al. [2008].

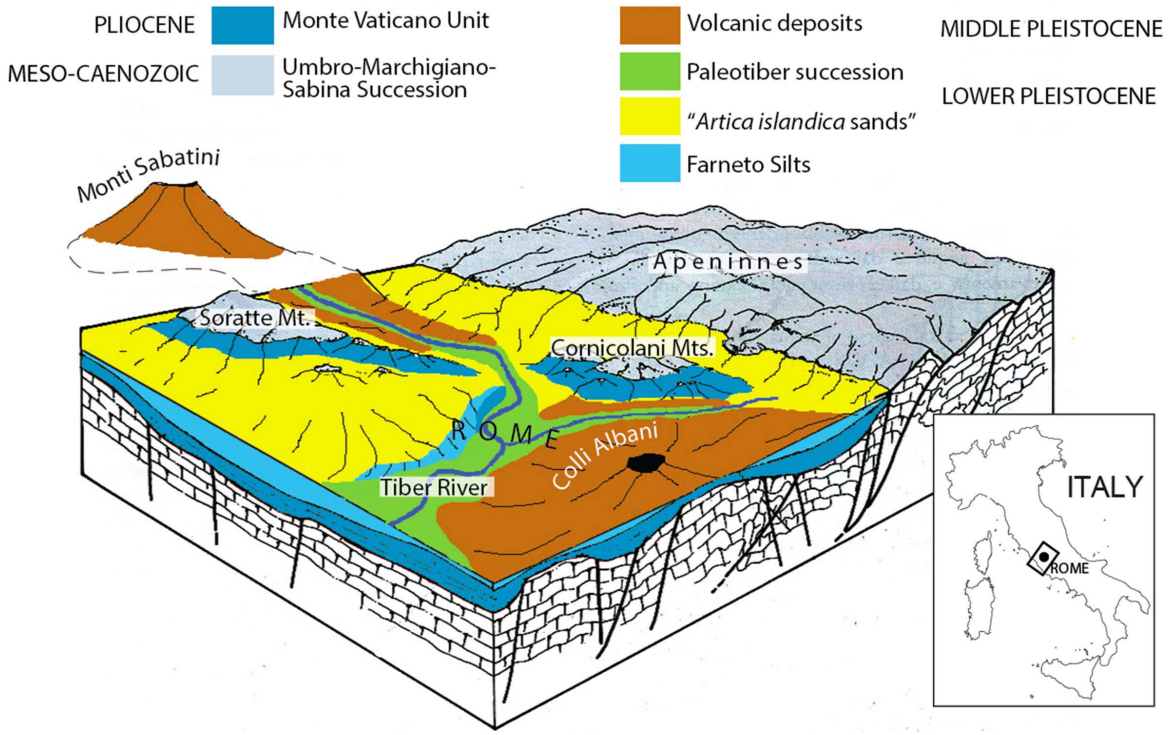


**Figure 2.** Snapshot of the paleogeographic and stratigraphic features of the area of Rome around 550 ka, at the beginning of the explosive activity occurred at the Monti Sabatini sand Colli Albani volcanic districts (modified from an original draft by Maurizio Parotto).

A well-defined hydrographic network, with valleys characterized by prominent and steep banks that delimit the alluvial plains, develops in the Rome area as a consequence of the tectonic uplift of about 50 m that occurred in the last 250 ka [Karner et al., 2001b; Marra et al., 2016b, 2019a, b]. These marked geomorphological characteristics, which at the end of the last glacial period gave rise to the tuffaceous cliffs that constitute the famous seven hills, are partially obliterated in the urban area, where over 2,000 years of anthropic activity have profoundly modified the original morphology, both through excavations, and with large thicknesses of fills to level out the depressions.

# 3. Stratigraphy

## 3.1 Aggradational Successions

The model of aggradational successions is the basis of the modern approach to the study of the geology of Rome [Luberti et al., 2017, and references therein]. This theoretical model is based on the observation that the sediments deposited near the coast in the Roman area since 1.3 Ma are always made up of fining-upwards sequences, generally with a coarse fraction (gravel) at the base, passing abruptly to the fine fraction (clay and, subordinately, sand) [e.g., Conato et al., 1980; Bellotti et al., 1994; Marra and Rosa, 1995; Karner and Marra, 1998, Marra et al., 2008]. The direct relationship between the fast rise of sea level and the deposition of a fining-upwards succession was known in the literature [e.g., Schumm, 1993]. The concept is based on the principle that a low sea level corresponds to a greater potential energy of the river system (difference in altitude between source and mouth) and therefore a greater transport capacity. As sea level rises, the transport capacity and therefore the grain size of the sedimentary material deposited by the river decreases (Fig. 3).

The continuous eruptive activity that occurred during the deposition of the aggradational successions determined that the pyroclastic products emitted by the volcanic districts of the Colli Albani and the Monti Sabatini were intercalated within these, providing the means to date, through the $^{40}Ar/^{39}Ar$ method, the sedimentary successions [Alvarez et al., 1996; Karner and Renne, 1998; Karner and Marra, 1998; Marra et al., 1998, 2008, 2016a, 2017a, 2021a, 2022; Marra and Florindo, 2014; Florindo et al., 2007; 2024; Pereira et al., 2020; Giaccio et al., 2021].

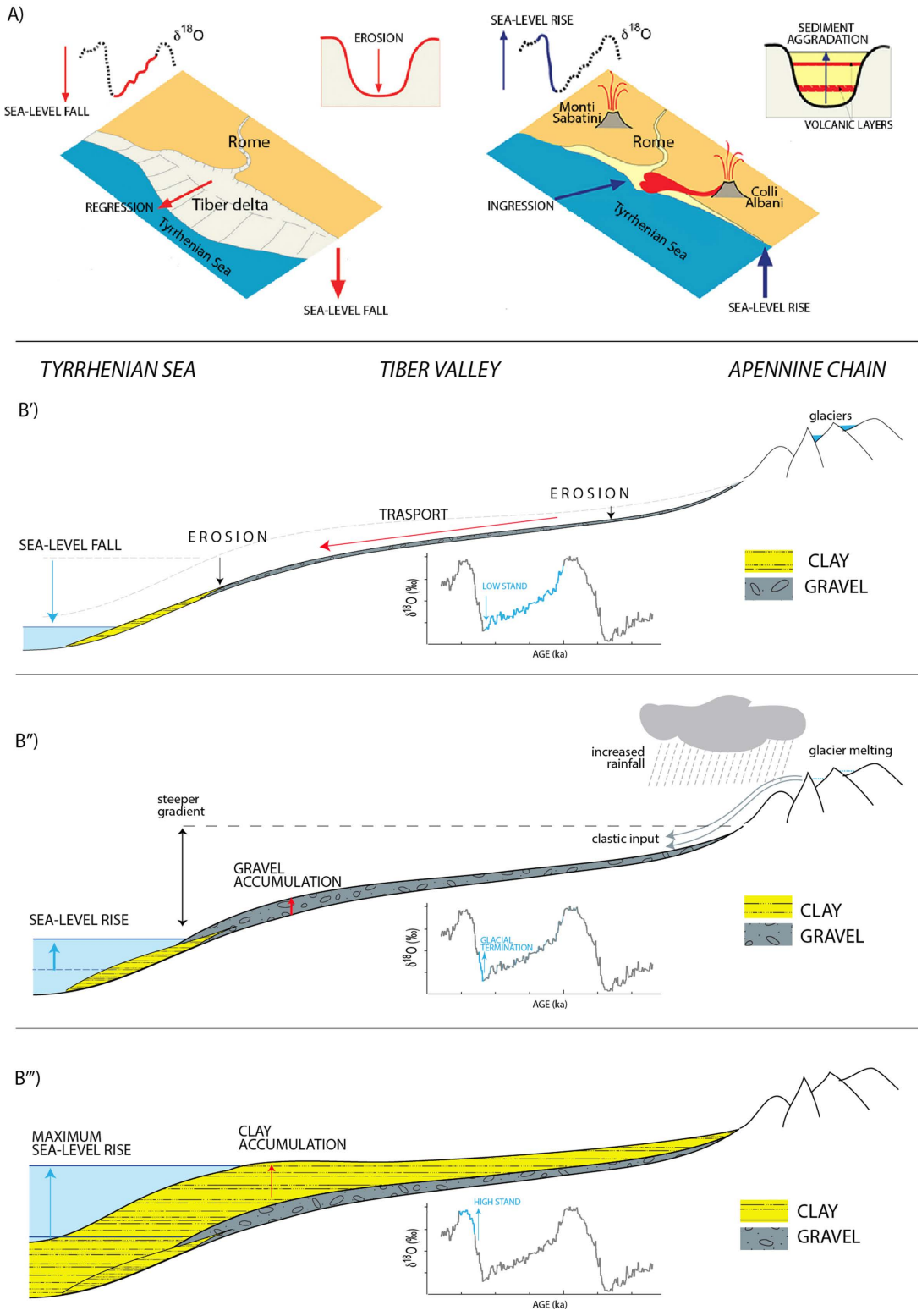


**Figure 3.** A: One aggradational succession is the sedimentary record deposited within the fluvial and coastal incisions excavated during periods of sea-level fall (glacial period), in response to sea-level rise at glacial terminations (interglacial period). B′-B‴: morpho-stratigraphic sketches showing how the conditions that make it possible to transport large quantities of gravel from the Apennines to the mouth of the Tiber occur only at the end of a glacial period, as a result of several concomitant factors:
i- maximum gradient along the river course due to the lowering of sea level that occurs during a glaciation;
ii- the end of the glaciation determines the melting of the glaciers with the consequent release of large quantities of water and, at the same time, of the gravelly materials originating from glacial erosion incorporated within them;
iii- strong increase in precipitation as a result of the increase in global temperatures.

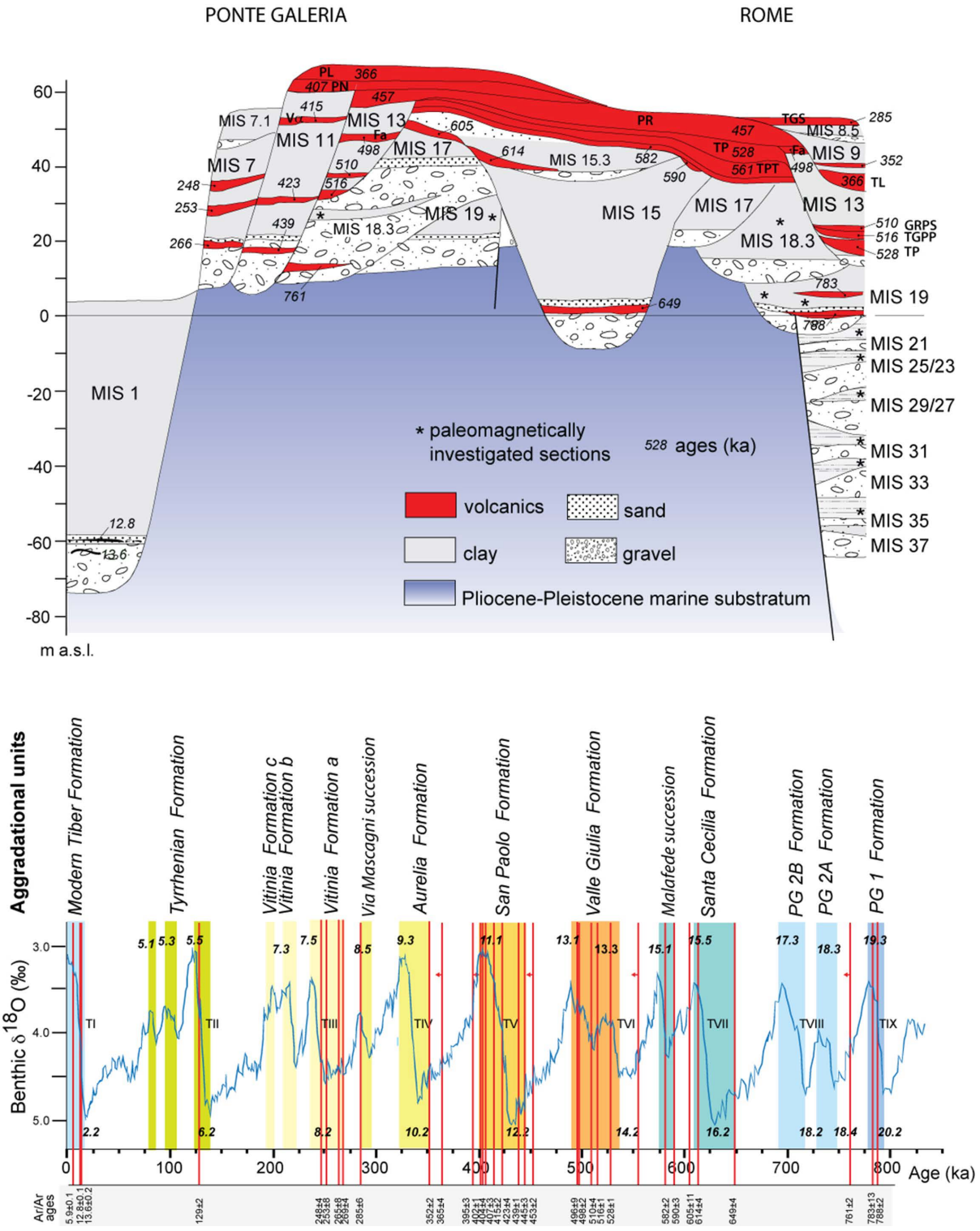


**Figure 4.** A: The scheme in the Figure represents an ideal overview of the aggradational successions in the Rome area and their morpho-stratigraphic relationships as a result of the interplay among glacio-eustatism, volcanic activity and tectonics. The different elevation at which we find the successions deposited in response to sea-level rise at different glacial terminations is a consequence of the progressive tectonic uplift and temporary phases of subsidence that characterized the Roman region throughout this period of time.

B: Colored boxes represent the aggradational phases corresponding to the deposition of the sedimentary successions in the area of Rome. Vertical red bars are the $^{40}Ar/^{39}Ar$ and $^{14}C$ age constraints providing correlation with the sea-level fluctuations as depicted in the Oxygen isotopes curve by Lisiecki and Raymo [2004]. Red arrows indicate *post-quem terminus* (maximum ages) for the glacial terminations.

Each aggradational succession is given a Formation name.

Dating of various aggradational successions has highlighted how the abrupt sedimentary transition between the basal gravels and clays, marked by a thin level of sand, is an excellent marker of glacial termination [Marra et al., 2008, 2013, 2016a]. It has in fact been understood that the transport of large quantities of gravel with pebbles up to 10 cm in diameter and their deposition in river and coastal sedimentary environments represents an exceptional fact, which presupposes very different hydrogeological conditions from the present (see Fig. 3), which were repeated only at particular moments in the past [Giaccio et al., 2021; Marra et al., 2022].

Over the years, all the aggradational successions deposited in the last 800 ka in the area between Rome and the coast have been reconstructed, thanks to the correlation and dating of numerous "aggradational sections" [Karner and Marra, 1988], both represented by outcrops and core drilling that have recovered the non-outcropping sedimentary successions. Each of the aggradational successions recognized in the Roman area has been correlated with a phase of sea-level rise at the end of each of the glaciations that occurred in the last million years, formally indicated with the number of the isotopic stage which preludes the glacial termination and with a "Formation" name, generally inherited from that of the successions already recognized in the geological literature (Fig. 4).

However, the stratigraphic nomenclature established in the literature based on this methodological approach has been neglected in the recent 1:50.000 geologic maps including the Rome's area realized by the CARG Project [Funiciello et al., 2008]. These maps adopt a nomenclature based on the Unconformity Bounded Stratigraphic Units (UBSU) system [Salvador, 1987] in which several Formations have been re-named, discarding the names previously introduced by the literature, while for some of them the $^{40}Ar/^{39}Ar$ dating has evidenced the incorrect chronostratigraphic position [see Luberti et al., 2017, for a detailed discussion]. In order to allow a correct correlation with the official geologic maps, a comparison between the stratigraphy adopted in the present work and that reported in the CARG maps for the geology of Rome is provided in Table 1.

| This work | | | | | CARG; Rome municipality maps (Funiciello and Giordano, 2008a; 2008b; 2008c; Funiciello et al., 2008) |
|---|---|---|---|---|---|
| MIS T | Age (ka) | Sedimentary unit | Volcanic unit | | |
| | | | Colli Albani | Sabatini [Vico] | |
| MIS 1 T-I | 18 – Present >12.8 <13.6 | **MT: Modern Tiber Fm** | | | **SFT$_b$** alluvial deposits |
| | 41±1 - 36±1 | | **Albano 2$^{nd}$ Eruptive Cycle:** Syn-eruptive lahar deposits 36±1-39±1<br>**Albano 7** 36±1<br>**Albano 6** (Peperino Albano) 36±1<br>**Albano 5** 39±1<br>**Albano 4** 41±1 | | ***TAL:*** *Tavolato Formation*(1)<br>*Via dei Laghi lithosome*(2)<br><br>***MNN$_a$:*** *Sandy-cobble lithofacies*<br><br>**UAL:** Albalonga Unit<br>**SDV:** Villa Doria Unit<br>**MNN:** Peperino Albano<br>**STL:** Cantone Unit |

(1) The "Tavolato Formation" was originally introduced by Fornaseri et al. [1963] as a volcaniclastic succession deriving from the reworking of the fallout and effusive deposits erupted during the final stages of the Villa Senni Eruption Cycle from a series of vents located along the peri-caldera fracture rim. It is therefore relatable to the MIS 9 aggradational succession (Aurelia Formation). Funiciello et al. [2008] have included in this formation the products of the eruptive activity of the Albano Crater, spanning 69-36 ka, as well as the "sandy-cobble lithofacies" that Funiciello et al. [2003] and De Benedetti et al. [2008] have interpreted as lahar deposits deriving from the overspill the Albano Crater Lake in Roman age, as well as the products of a supposed Holocene eruptive activity. However, a wide dataset of $^{40}Ar$-$^{39}Ar$ dating consistently indicates that the last documented eruptive event occurred at the Albano maar 36 ka [Marra et al. 2003; Freda et al., 2006; Giaccio et al., 2007, 2009], in spite of younger ages reported in the literature [e.g., ~26 ka; Villa et al., 1999] that are affected by stratigraphic inconsistencies and/or methodological uncertainties. As a matter of fact, young radiocarbon ages of ca. 5 ka on bulk soil samples underlying these lahars, have shown to be unreliable ones [Giaccio et al., 2009]. Moreover, historic, archaeologic, hydraulic and engineering analyses of the ancient Latin sources and of the lake emissary tunnel proved that the lake level was 70 m lower than the crater rim also in Roman epoch, hindering the water overspill [D'Ambrosio et al., 2010]. For these reasons, the occurrence of volcanic activity and lahar deposition from the Albano Crater in Roman times is devoid of scientific evidence, and the sandy-cobble lithofacies must be considered as deriving from the syn-eruptive, or shortly post-eruptive, volcaniclastic sedimentation occurred around 36 ka [Freda et al., 2006; Giaccio et al., 2007, 2009].

(2) The "Via dei Laghi lithosome" includes a number of phreatomagmatic vents of different age, spanning the late Villa Senni Eruption Cycle (e.g., Castiglione and Pantano Secco craters) to the latest Hydromagmatic phase (e.g., Albano second eruption cycle), 365 through 36 ka.

| This work | | | | | CARG; Rome municipality maps (Funiciello and Giordano, 2008a; 2008b; 2008c; Funiciello et al., 2008) |
|---|---|---|---|---|---|
| MIS T | Age (ka) | Sedimentary unit | Volcanic unit | | |
| | | | Colli Albani | Sabatini [Vico] | |
| | 69±1 | | **Albano 1st Eruptive Cycle:**<br>**Albano 3** 69±1<br>**Albano 2**<br>**Albano 1** 69±1 | | **KRL:** Corona del Lago Unit<br>**DSN:** Coste dei Laghi Unit<br>**TGO:** Montagnaccio Unit |
| | 69 ka-? | | **Giuturna Eruptive Center** | | **PVN:** Pavona Unit<br>**KLG:** Quarto Laghetto Unit |
| | | | | **Martignano** 70±3<br>**Piana dei Falliti** 89±12<br>**Baccano Upper Unit** 91±6<br>**Baccano Main Unit** *85±9*<br>**Le Cese** 95±5<br>**Stracciacappa** 97±4 | **UDM:** Martignano Unit<br>**$BCC_3$:** Baccano Upper Unit<br>**$BCC_2$:** Baccano Ignimbrite<br>**CPP:** Stracciacappe Unit<br>**PLL:** Polline Unit; **LCC:** Conca Unit |
| | 102±2 | | **Valle Marciana Eruptive center** | | **MAK:** Valle Marciana Unit |
| MIS 5.5/5.1 T-II<br>MIS 5.1<br>MIS 5.3<br>MIS 5.5 | 133-79<br>>130±2<br><144±1 | **TY: Tyrrhenian Fm**<br>Linguadoca sub-unit<br>Monte Carnevale sub-unit<br>Cava Rinaldi sub-unit | | **Baccano Lower Unit** 131±2 | **RDM:** Riserva della Macchia Unit<br>**TSV:** Tenuta di Campo Selva Unit<br>**$BCC_1$:** Baccano Lower Unit |
| | 150±6-142±4 | | **Nemi Eruptive center** | | **NEM:** Nemi Unit |
| | 204±2-201±2 | | **Ariccia Eruptive center** | | **ICA:** Ariccia Unit |
| 8.4/7.1 T-III | 269-194<br>≥248±4 | **VT: Vitinia Fm** | **Monte delle Faete Phase** 308±4 - 241±5<br>**Capo di Bove lava** 277±2<br>**Saponara lava** 277±2<br>**Prata Porci Eruptive center** 279±6 | **TPP: Tufo di Pizzo Prato** 249±16<br>**Vigna di Valle lava** 283±6<br>**TGS: Tufo Giallo di Sacrofano** 285±2 | **VTN:** Vitinia Formation;<br>***SKP:*** *Saccopastore Unit*(3)<br>**$VDV_1$:** Pizzo Prato Unit<br>**PRK:** Prata Porci Unit<br>**VDV:** Vigna di Valle Lava Unit<br>***NMT:*** *Via Nomentana Unit* |
| 8.5 | 295-285 | **VM: Via Mascagni succession** | | | |
| 9.3 T-IV | 355-325<br>≥345±2 | **AU: Aurelia Fm** | | | **AEL:** Aurelia Formation;<br>**CLZ:** Castelporziano Unit;<br>**VSN:** Pebbly-sandy lithofacies;<br>**NCF:** Nuova California Unit |

(3) The Saccopastore Unit, in which two skulls of Neanderthal individuals were recovered [Sergi, 1929], was attributed to the Tyrrhenian Stage (i.e., MIS 5.5) based on a by now superseded subdivision of the glacial epochs [Blanc, 1939]. However, based on the geometry, elevation and sedimentologic features of the sedimentary deposits, Marra et al. [2015a] have correlated the gravel layer hosting the human remains with glacial termination III at the onset of MIS 7 and attributed the aggradational succession cropping out in Saccopastore to the Vitinia Formation, suggesting an age of ~245 ka for the Neanderthal remains.

| This work | | | | | CARG; Rome municipality maps (Funiciello and Giordano, 2008a; 2008b; 2008c; Funiciello et al., 2008) |
|---|---|---|---|---|---|
| MIS T | Age (ka) | Sedimentary unit | Volcanic unit | | |
| | | | Colli Albani | Sabatini [Vico] | |
| | 365±4-351±4 | | **Villa Senni Eruptive Cycle: Madonna d. Angeli succ.** 364±3 - 351±4 **Castiglione Eruptive Center Pantano Secco Er. center** 364±1 **PL: Pozzolanelle TL: Tufo Lionato** 365±4 | | **FKB:** Madonna degli Angeli Formation<br>**PSK:** Pantano Secco Unit<br>Villa Senni Formation:<br>**$VSN_2$:** Pozzolanelle<br>**$VSN_1$:** Tufo Lionato |
| | | | | **SA: Sant' Abbondio Succession** 387±4 [**Vico β** 406±3] [**Vico α** 415±2] | ***LTT:*** *Tufi Stratificati Varicolori di La Storta*(4) |
| | 407±2 - 398±5 | | **Pozzolane Nere E.C.: Fontana Centogocce succ.** 404±5 - 398±5 **PN: Pozzolane Nere** 407±2 **FL: Fioranello Lava** | | **$SLV_b$:** Fontana Centogocce Formation<br>**PNR:** Pozzolane Nere<br>**RMN:** Fosso Tre Rami Lava Unit |
| 11.3 T-V | 450-402 >423±4 <439±1 | **SP: San Paolo Fm** | | | ***FTR:*** *Fosso del Torrino Formation*(5); **$FTR_1$:** Conglomerato Giallo |
| | | | | **Tufo Rosso a Scorie Nere E. C.: Fall F** 444±7 **Fall E** 447±7 **TRSN: Tufo Rosso a Scorie Nere** 449±2 **Fall D** | **RNR:** Tufo Rosso a Scorie Nere |
| | 457±5 - 441±5 | | **Pozzolane Rosse E. C.: Corcolle succession** 456±3-441±5 **PR: Pozzolane Rosse** 456±3 **VL: Vallerano lava** 457±5 | | **RED:** Pozzolane Rosse<br>**LLL:** Lave di Vallerano |
| 13.3/13.1 T-VI | 550-490 >528±1 <551±5 | **VG: Valle Giulia Fm** | **AF: Ash-fall Succession** 517±1-500±3 | **TTPB: Tufi Terrosi con Pomici Bianche: Fall C** 461±2 **Fall B** 490±14 **Fall A** 496±3 - 493±9 **GRPS: Grottarossa Pyrocl. Seq.** 508±9 **TGPP: T. Giallo di Prima Porta** 514±6 | **VGU:** Valle Giulia Formation ***SKF:*** *Tufi Stratificati Varicolori di Sacrofano*(4)<br>**PPT:** Prima Porta Unit |

(4) The "Tufi stratificati varicolori di Sacrofano" [De Rita et al., 1983] and "Tufi stratificati varicolori di La Storta" [Corda et al., 1978] are two superseded formation names which grouped the undifferentiated successions of volcanic and intercalated lacustrine deposits comprised between the eruptions of "Tufo Giallo della Via Tiberina" and "Tufo Roso a Scorie Nere", and between "Tufo Rosso a Scorie Nete" and "Tufo Giallo di Sacrofano", respectively [Karner et al., 2001].

(5) "Fosso cel Torrino", "Casale del Cavaliere", and "Tor de' Cenci" are unjustified re-naming of the previously formalized San Paolo Formation [Marra and Rosa, 1995], Tufo di Acque Albule, and Tufo Pisolitico di Trigoria [Karner et al., 2001a, 2006].

| This work | | | | | CARG; Rome municipality maps (Funiciello and Giordano, 2008a; 2008b; 2008c; Funiciello et al., 2008) |
|---|---|---|---|---|---|
| MIS T | Age (ka) | Sedimentary unit | Volcanic unit | | |
| | | | Colli Albani | Sabatini [Vico] | |
| | 528±1 - 527±2 | | **Tufo del Palatino E.C.:**<br>**TAA: Tufo di Acque Albule** 527±2<br>**TP: Tufo del Palatino** 530±2 | | ***KKA:*** *Casale del Cavaliere Unit*(5)<br>**PTI:** Palatino Unit |
| | 546±3 | | | **Tufo Giallo d. Via Tiberina E. C.**<br>**TGVT: T. Giallo d. Via Tiberina** 543±3<br>**FAD 3** 543±5 (21)<br>**FAD 2** 554±14; 561±3 | **TIB:** Via Tiberina Unit |
| | 561±2 - 555±1 | | **T. Pisolitico di Trigoria E. C.:**<br>**TPT: Tufo Pisolitico di Trigoria** 561±2 | | ***DC:*** *Tor de' Cenci Unit*(5) |
| 15.2/15.1<br>T-VIIB | 614-590<br>612±6 | **FM: Fosso di Malafede succession** | | **Castelnuovo di Porto Eruptive Cycle:**<br>**FAD 1**<br>**TGCP: Tufo Giallo di Castelnuovo di Porto** 585±4<br>**FAD 0** 585±2 | |
| 15.5<br>T-VIIA | 650-625<br>649±3 | **SC: Santa Cecilia Fm** | | **Santa Cecilia Eruption Unit** 611±3<br>**Vigna Murata Eruption Unit** 649±4 | **CIL:** Santa Cecilia Formation;<br>**$PGL_{3c}$**: Sandy Litho-facies;<br>***FCZ:*** *Fosso della Crescenza Formation*(6) |
| 17.3<br>T-VIIIB | 729-700<br>≤*729±19* | **PG2: Ponte Galeria 2 Fm:**<br>PG2B succession<br>*Venerupis senescens* clay<br>Gravel and sand<br>with frequent cross-laminations | | | **PGL:** Ponte Galeria Formation<br>**$PGL_3$**: Pisana Member<br>**$PGL_{3b}$**: Sandy-clay Lithofacies<br>**$PGL_{3a}$**: Conglomerate-sandy Litho-facies |
| 18.3<br>T-VIIIA | 761-729<br>≤761±2 | PG2A succession<br>Middle clay<br>Gravel and sand<br>with frequent cross-laminations | | **Ponte Galeria Eruption Unit** 761±2 | |
| 19.3<br>T-IX<br>? | 790-782<br>≥788±2<br>? | **PT1: Paleotiber 1 Fm**<br>**PG1: Ponte Galeria 1 Fm:**<br>*Helicella* clay<br>River conglomerate | | **Paleotiber Succession:**<br>**Unit D** 783±13<br>**Unit C** *796±9*<br>**Unit B** *800±9*<br>**Unit A** 788±2 | **$PGL_2$**: Argille ad Helicella Auctt.<br>**$PGL_1$**: Conglomerati di Casale dell'Infernaccio |
| 37-21 | ≥807<br>≤1318 | **PTG: Paleotiber Graben Fm/MP: Monte delle Piche Fm**<br>including at the base:<br>**MC: Monte Ciocci Fm**<br>(MIS 37) | | | **MDP:** Monte delle Piche Formation<br>Clayey-sand Lithofacies **PGLb**<br>Conglomerate Lithofacies **PGLa** |

(5) "Fosso cel Torrino", "Casale del Cavaliere", and "Tor de' Cenci" are unjustified re-naming of the previously formalized San Paolo Formation [Marra and Rosa, 1995], Tufo di Acque Albule, and Tufo Pisolitico di Trigoria [Karner et al., 2001a, 2006].

(6) "Fosso della Crescenza Formation" lacks geochronologic constraints allowing to correlate it with the Santa Cecilia Formation (in which case a distinct name would be redundant), nor any other formation.

| This work | | | | | CARG; Rome municipality maps (Funiciello and Giordano, 2008a; 2008b; 2008c; Funiciello et al., 2008) |
|---|---|---|---|---|---|
| MIS T | Age (ka) | Sedimentary unit | Volcanic unit | | |
| | | | Colli Albani | Sabatini [Vico] | |
| 56/55 | 1628-1585 | **MM: Monte Mario Fm:** *Cerastoderma* clay Yellow sands with silty intercalations | | | **MTM:** Monte Mario Formation |
| 58/57 | 1660-1628 | Yellow sands with "panchina" *Arctica islandica* sands Farneto silts | | | **$MTM_1$:** Farneto Member |
| ZANCLEAN | 3810-2700 | **MV: Monte Vaticano Fm** | | | **MVA:** Monte Vaticano Formation |

**Table 1.** Stratigraphic nomenclature [modified from Luberti et al., 2017]. The first column reports the marine isotopic stage (MIS) and the glacial termination (T) which the aggradational successions are correlated to. The age constraints achieved in Rome for the correlation are reported in the second column. The formal name of the sedimentary and volcanic units adopted in the present study are reported in the third, fourth and fifth column. The corresponding unit and formation names of the official geologic maps realized by the CARG Project are in the sixth column; the formation names which are redundant with previously introduced names or superseded by more detailed and correct stratigraphic nomenclature are reported in italics.

## 3.2 Volcanic Stratigraphy

Due to the prescriptions imposed by the Soprintendenza Archeologica and to those deriving from the dense network of subsurface facilities on the location of the performed boreholes, none of them encountered the volcanic deposits which constitute the uppermost geologic horizon in the historical center of Rome. However, detailed information on the volcanic stratigraphy in this area has been achieved in several outcrops and by a number of direct observations of boreholes performed for civil engineering purpose in the last years (see Fig. 5 for location), combined with a few detailed reports from literature [De Angelis D'Ossat, 1938, 1948]. A dedicated borehole though the volcanic cover is planned in the second phase of the Predict Project, aimed at performing in situ geophysical measurements.

A synopsis of the volcanic units occurring in the central area of Rome and their stratigraphic relationships with the aggradational successions deposited in the time span 589-200 ka is shown in Figure 6. A complete overview of the volcanic units of the greater area of Rome and their nomenclature is provided in Table 1.

Here we briefly describe the deposits erupted by the Colli Albani, Monti Sabatini and, subordinately, Vico volcanic districts, that are present in central Rome; for their detailed textural, compositional and petrochemical features we remand the readers to Karner et al., 2001a; Sottili et al., 2004, 2010; Giordano et al., 2006; Marra et al., 2009, 2011, 2014; Boari et al., 2009; Gaeta et al., 2006, 2016.

*Colli Albani*

The Colli Albani volcanic products occurring in central Rome are those erupted during the Tuscolano-Artemisio (T-A) phase [De Rita et al. 1988; 1995], which are characterized by low $SiO_2$ ($\leq$45 wt.%) and by a modal assemblage consisting of clinopyroxene and leucite, with accessory biotite, ranging in composition from K-foidite to tephrite [Gaeta et al., 2016, and ref. therein]. The T-A phase produced five geochronologically distinct, large Eruption Cycles (E.C.) in the time span 561-365 ka [Karner et al. 2001a; Marra et al. 2009; Gaeta et al., 2016], accompanied by minor hydromagmatic, strombolian and effusive activity. An early phase of activity, which included the Tufo Pisolitico di Trigoria E.C. and the Tufo del Palatino – Tufo di Acque Albule E.C., was characterized by hydromagmatic features [Palladino et al., 2001]. The pyroclastic-flow deposits of these three eruptions in central Rome display similar macroscopic textural aspect: they are dark grey, "granular" (matrix-supported lapilli-sized scoriae and loose leucite, pyroxene and biotite crystals), semi-lithified, often thinly laminated, few cm- to several m-thick deposits.

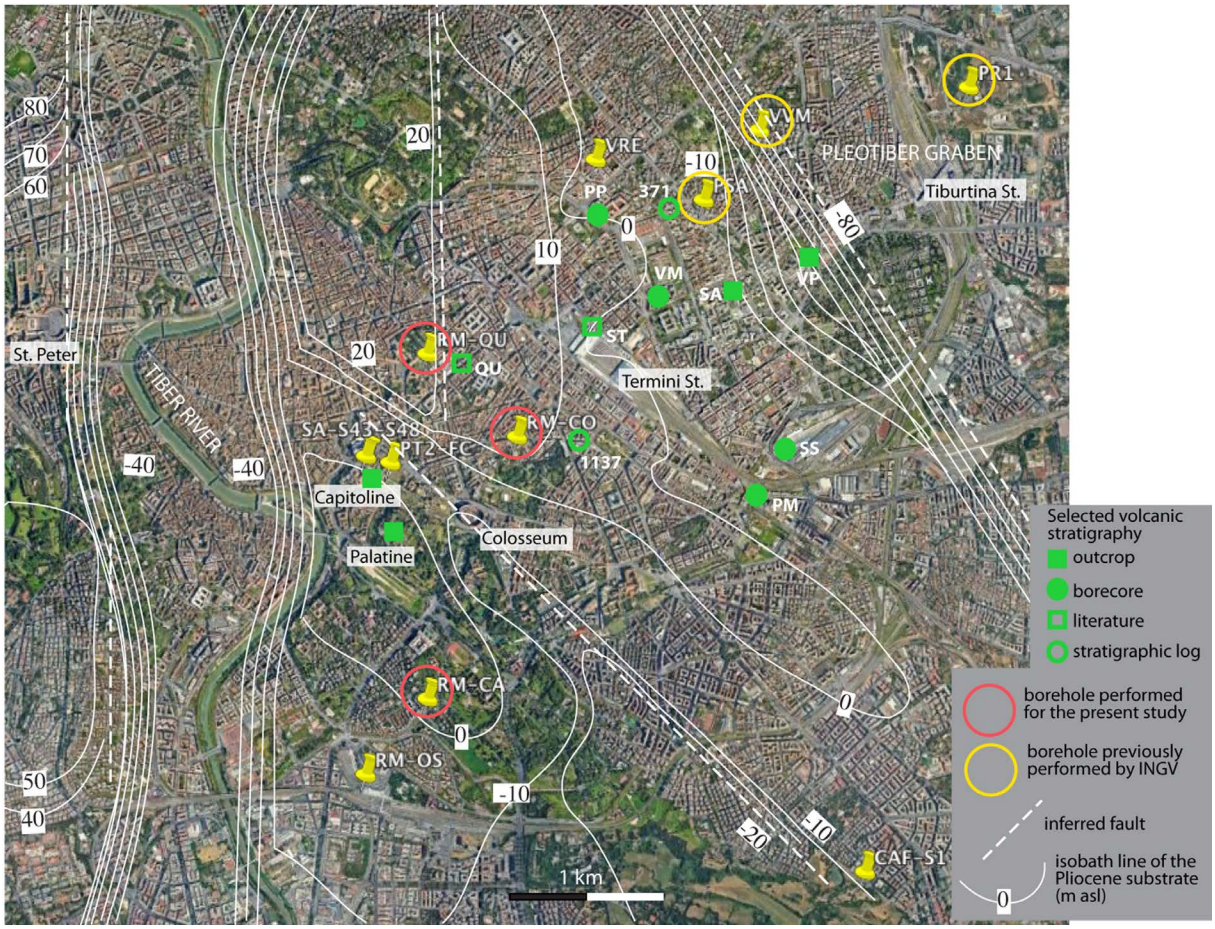


**Figure 5.** Satellite image of the City of Rome showing location of the boreholes and outcrops described in the present work. The elevation (in m asl) of the sedimentary marine "bedrock" is also shown [modified from Marra and Florindo, 2014].

The following E.C.'s produced larger pyroclastic eruptions with a drier character, emplacing three huge, massive ash-and-scoria flows (pozzolan): the Pozzolane Rosse (456 ± 4 ka) and Pozzolane Nere (407 ± 3 ka) pyroclastic flows and the Villa Senni Eruptive Sequence (365 ± 4 ka), which includes a lithified, welded facies emplaced within the paleo-incision in the early stages of the eruption, (Tufo Lionato), followed by an incoherent facies (Pozzolanelle) [Freda et al. 1997].

Thick paleosols separate these pyroclastic-flow deposits affecting also the overlying fallout ash deposit which emplaced in the intervening time span. Such fallout deposits are constituted only minimally by the post-caldera activity which followed the explosive eruptions occurred at Colli Albani, while for the most part they are wind-blown from the Monti Sabatini, in consequence of the regional westerly winds.

For the same reason, the products of the strombolian and moderately explosive hydromagmatic activity occurred during the Faete Phase [308-250 ka, Karner et al., 2001a; Marra et al., 2003; Gaeta et al., 2016] and the Late phreatomagmatic phase [200-36 ka; Marra et al., 2003, 2016; Freda et al., 2006; Giaccio et al., 2009; Gaeta et al., 2011] are lacking in central Rome, while the Capo di Bove lava flow (277 ka) and the Peperino Albano pyroclastic flow (36 ka) reached only the south-eastern outskirt of the City.

*Monti Sabatini Volcanic District*

With respect to the Colli Albani, the Monti Sabatini explosive products have a higher $SiO_2$ content (≥ 50 wt.%), spanning in composition from trachytes to phonolites, display a higher degree of vesiculation of the scoria (pumice), and are characterized by a mineralogical assemblage of sanidine, leucite, and clinopyroxene [Scherillo 1947; Conticelli et al. 1997; Sottili et al. 2004; Masotta et al. 2010].

Only the products of the early highly explosive activity [ca. 582 to 490 ka, Marra et al., 2014, 2017a, 2020] which took place at the Morlupo and at the Southern Sabatini centers [Sottili et al. 2004] are present in central Rome, while

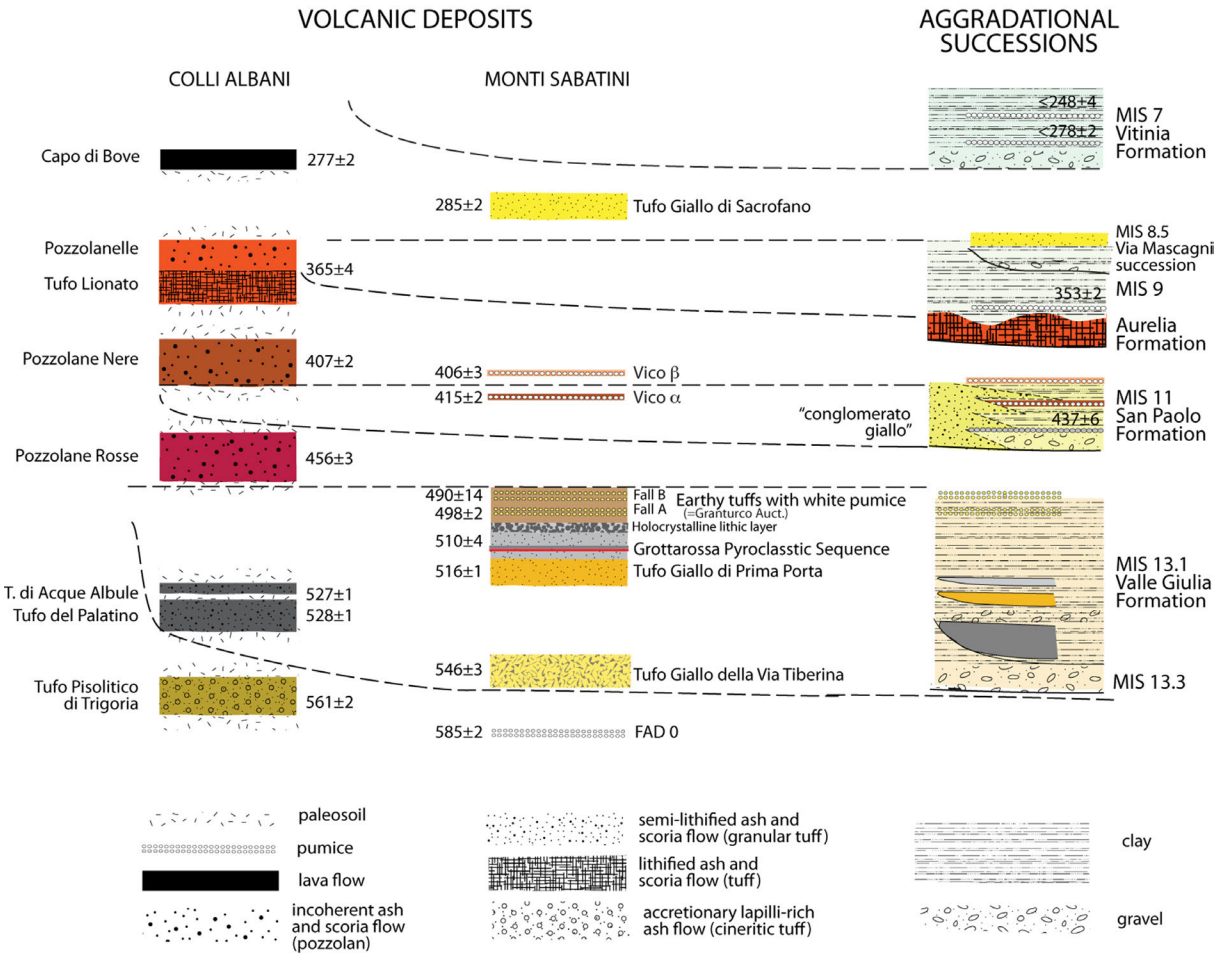


**Figure 6.** Stratigraphic columns showing the volcanic products occurring in Rome and their relationships with the coeval aggradational successions. The $^{40}Ar/^{39}Ar$ ages (in ka) from literature (see text) of all the dated products are reported.

the Tufo Giallo di Sacrofano pyroclastic-flow deposit [285 ± 2 ka, Karner et al., 2001a, Sottili et al., 2010] reached the northern hinterland, where it overlies the fluvial-lacustrine deposits of the MIS 8.5 aggradational succession [Via Mascagni succession, Marra et al., 2017b].

Such activity was characterized by huge pyroclastic flows and subplinian to plinian fallout deposits. In Rome, the First Ashfall Deposits (FAD 0, 582 ± 2 ka) represent the earliest volcanic deposit above the Paleotiber successions and are interbedded with the sedimentary deposit of the late MIS 15.1 aggradational succession [Fosso di Malafede succession, Marra et al., 2009; Marra and Florindo, 2014] underlying the Tufo Pisolitico di Trigoria (561 ± 1 ka).

The distal pyroclastic-flow deposits of Tufo Giallo della Via Tiberina (546 ± 3 ka), Tufo Giallo di Prima Porta (516 ± 1 ka) and Grottarossa Pyroclastic Sequence (510 ± 4 ka) reached the center of Rome flowing along the Tiber River Valley, while thinner overbank facies and subordinated ash-fall and scoria-fall deposits emplaced on the morphological heights.

Subsequently, a new eruptive phase took place at the southern Sabatini volcanic centre emplacing the thick succession of Tufi Terrosi con Pomici Bianche fallout deposits [Karner et al., 2001a; Sottili et al., 2004], which in Rome are constituted by an up to four meters thick succession of very altered ash, with the intercalation of two discontinuous, up to 30 cm thick pumice fallouts (Fall A, 498 ± 2 ka, and Fall B, 590 ± 14 ka), known with the local name of *Granturco* [Fornaseri et al. 1963].

### *Vico*

A highly explosive eruptive phase took place at the Vico volcano 415 through 400 ka [Cioni et al., 1993; Perini et al., 2004; Pereira et al., 2020], coincident with a dormancy period occurred at the Monti Sabatini district [Marra et al., 2020]. The plinian pumice fallout deposit of Vico α (415 ± 2 ka) are intercalated with the sediments of

San Paolo Formation in central Rome [Karner et al., 2001a], while those of Vico β (406 ± 3 ka) have been identified by Marra et al. [2015b] in the stratigraphy of the excavations at Termini Station described in De Angelis D'Ossat [1948].

# 4. Methods

## 4.1 Boreholes

Three boreholes (RM-QU, RM-CO, RM-CA) have been planned in key points of the historical center of Rome, aimed at recovering the full stratigraphic record comprised between the ground surface and the Pliocene marine substrate (Fig. 5). Such substrate has been considered as the seismic "bedrock" in the early works that have attempted at assessing the seismic response in Rome [e.g., Rovelli et al., 1994, 1995], while a major role played by the gravel horizon occurring above it in increasing the p-wave and s-wave velocity has been more recently highlighted [Caserta et al., 2013]. Previous work has evidenced that the basal gravel horizon of the Paleotiber successions displays sub-horizontal attitude in discrete sectors that occur at different elevation asl, in consequence of the different sedimentary cycles associated with the glacio-eustatic fluctuations and possible intervening tectonic dislocation [Marra and Rosa, 1995; Marra and Florindo, 2014]. The boreholes have been located in three sectors characterized by different elevation of the basal gravel horizon, aimed at providing age constraints through the detrital sanidine dating method and recognize different sedimentary successions and/or their fault displacement. Moreover, the information provided by the scheduled boreholes has been implemented through a set of other borecores recovered from previously performed drillings in several areas of Rome (Fig. 5). These include the complete coring record of a 50 m-deep borehole drilled in the Caffarella Valley to the south east of the urban area (CAF-S1), a core segment of the grey clay of the Paleotiber succession from north Rome (VRE), five samples collected from three boreholes drilled at the Capitoline Hill provided by the Soprintendenza Capitolina (SA, S43, S48), and one gravel sample collected at the Fori Imperiali (PT2-FC).

Detailed stratigraphic logs of the three boreholoes performed by INGV are provided in Supplementary Material #1.

## 4.2 $^{40}Ar/^{39}Ar$ dating

### 4.2.1 Detrital Sanidine Method

The volcanic activity of the districts of the Roman Province becomes extremely intense and continuous starting from around 600 ka; in addition to providing a means of direct dating of the sedimentary successions in which its products are densely intercalated, this eruptive activity has allowed the development and application of an innovative dating method, based on the age of individual reworked sanidine crystals, contained within a sedimentary deposit [detrital sanidine; see Marra et al., 2019b for an in depth discussion].

The extensive application of this method in the Latium region has shown that, in addition to providing a maximum age for the sediment (*terminus post-quem*), the age of the youngest crystal (or crystal population) can also be considered a *terminus ante-quem* for deposition time, providing an absolute, yet approximate age constraint. This assumption is based on the fact that volcanic activity was very intense and continuous in this period and by dating a significant number of crystals in a sample (e.g. 30) the probability that crystals from the most recent eruption which occurred up to the moment of deposition are not represented is statistically low. This derives from the fact that the latest eruption crops out more extensively than the previous ones and is more susceptible to being eroded and included in the sediment. And since the eruptive activity was continuous on the scale of millennia, the absence of younger crystals can be considered evidence of a deposition that occurred in the time interval separating two subsequent eruptions.

This method proved to be particularly effective in the interval 600-200 ka, when the activity of the Latium volcanoes was more intense and continuous, while it must be used with caution, as an indicator of maximum age, in the interval between 1300 and 800 ka and between 200 ka and the Present in this region.

Within the Predict project, we planned to use the detrital sanidine method to provide age constraints to the Paleotiber successions deposited in the interval 800-600 ka, in which the presence of primary volcanic layers is rare.

The dating of 8 samples of gravel and sand collected from the borecores is ongoing at the Wiscar Laboratory of the University of Madison, Wisconsin. Here we present unpublished data on three gravel samples collected at the Fori Imperiali (PT2-FC), The Capitoline Hill (S48-C3-11.6) and Monte Ciocci (PT1-MC6) in the Paleotiber aggradational successions occurring in central Rome, in the Paleotiber delta, and in the Monte Mario-Gianicolo structural height, respectively, aimed at verifying their correlation with the MIS's of the Oxygen isotope timescale. Moreover, we have re-dated the Tufo del Palatino on a sample collected at the Capitoline Hill (TP-CH).

#### 4.2.2 $^{40}Ar/^{39}Ar$ analysis

Sanidine phenocrysts were leached in 3M HCl for twenty minutes, rinsed repeatedly with deionized water, and then leached in 10% HF for ten minutes followed by additional water rinses. The purified separates were co-irradiated with the 1.1864 Ma Alder Creek sanidine standard [Jicha et al., 2016] at the Oregon State University TRIGA reactor in the Cadmium-Lined In-Core Irradiation Tube. Single crystal fusion analyses were conducted at the WiscAr laboratory at the University of Wisconsin-Madison, utilizing a 55W $CO_2$ laser and a Noblesse multi-collector mass spectrometer, according to Jicha et al. [2016]. All of the $^{40}Ar/^{39}Ar$ ages are calculated using the decay constants of Min et al. [2000] and are reported with 2σ analytical uncertainties, including the J uncertainty. The full analytical data are reported in Supplementary Material #2.

### 4.3 Paleomagnetism

For aggradational successions older than 600 ka, in addition to the rare geochronological constraints provided by the intercalations of the first volcanic products, a further relative dating method was used, represented by magnetostratigraphy on clayey successions. Magnetostratigraphy is a technique that uses the record of the polarity reversals of the Earth's magnetic field registered in sedimentary and/or volcanic rocks as a correlation and dating tool [e.g., Opdyke and Channel, 1996; Langereis et al., 2010]. The Quaternary Period, the most recent part of which we focus on in this study, is characterized by ten main polarity reversals, from the top of the Gauss Chron (2610 ka) to the Matuyama-Brunhes reversal (773 ka) [Geomagnetic Instability Time Scale, Singer, 2014].

Paleomagnetism proved particularly valuable in determining the age of the aggradational successions deposited during this period in the ancient Paleotiber delta [Florindo and Marra, 1995; Marra et al., 1998; Florindo et al., 2007; Marra and Florindo, 2014; Florindo et al., 2024]. Additionally, in combination with $^{40}Ar/^{39}Ar$ dating, paleomagnetism aided in dating successions aged between 800 and 600 ka, which are extensively exposed between Rome and the current coast in the Ponte Galeria area (Fig. 4).

In this work, we present preliminary results of the paleomagnetic investigation conducted on the RM-CO, as well as on core segment VRE. The aim of these investigations is to temporally place these stratigraphic intervals relative to the Matuyama-Brunhes boundary.

We present the demagnetization of the samples, resulting in the definition of the Characteristic component of NRM (ChRMs). The choice of the most suitable demagnetization method stems from our experience in the paleomagnetic study of these sedimentary sequences in the Rome area [Florindo and Marra, 1995; Marra et al., 1998; Florindo et al., 2007; Marra and Florindo, 2014; Florindo et al., 2024].

From our previous studies it is evident that the primary mineral responsible for the magnetic signal within these sedimentary sequences is magnetite, occasionally accompanied by greigite in certain intervals. A series of new mineral magnetic analyses, based on magnetic coercivity and thermal unblocking characteristics, is currently underway to determine changes in magnetic mineral composition, concentration, and grain size throughout these units. This will be the focus of a companion paper.

#### 4.3.1 Paleomagnetic Sampling, Laboratory Procedures and Analysis

The 20 m thick clay section recovered in borehole RM-CO was sampled for paleomagnetism from 16.74 to 34.40 m depth (29.26-11.60 m asl) using standard 8 $cm^3$ plastic cubes. Eleven samples were collected from the center of the splitcore sections, as this is less affected by coring disturbance and all samples were oriented with respect to vertical.

Lack of azimuthal orientation did not pose a problem for polarity determination because the geomagnetic field at the latitude of this site (42°N) has a steep inclination (± 61assuming a geocentric axial dipole field).

To ensure minimal sample dehydration and alteration, we placed the samples in sealed bags and stored them in a refrigerated room until processing. As in our previous studies, the natural remanent magnetization (NRM) of all samples was analyzed in the magnetically shielded paleomagnetic laboratory at the INGV, Rome, using a 2-G Enterprises (model 755) narrow-access pass-through cryogenic magnetometer, with in-line AF demagnetization capability.

The NRM was stepwise AF demagnetized at successive peak fields of 4, 8, 13, 17, 21, 25, 30, 35, 40, 45, 50, 60, 80, and 100 mT. Demagnetization data were examined using orthogonal vector component diagrams, stereographic projections, and intensity decay curves. We determined characteristic remanent magnetization (ChRM) directions by using principal component analysis (PCA) with linear best fits calculated from four or more demagnetization steps, using the PuffinPlot paleomagnetic analysis application developed by Lurcock and Florindo [2019]. For each sample, we utilized two options for PCA analysis: (a) the free option, where the line is fitted through the data without the constraint of passing through the origin of orthogonal demagnetization diagrams, and (b) the anchored option, where the line is also fitted through the data but is anchored to the origin of orthogonal demagnetization diagrams. Case-by-case, we decided on the most appropriate approach.

*Borehole VRE*

Four samples were collected from a 50 cm-long fine-grained core segment previously recovered in borehole VRE to verify its possible temporal correspondence with a clayey section exhibiting inverse magnetic polarity, recovered in borehole PSA [Florindo et al., 2007].

We obtained samples at a depth between 28.70 and 29.20 meters (16.30-15.80 m asl) by drilling conventional cylindrical paleomagnetic samples (25 mm diameter and 22 mm height) using a gasoline-powered hand drill with a water-cooled diamond bit. Similar to borecore RM-CO, this core was not azimuthally oriented, and all samples were oriented with respect to vertical to facilitate polarity determinations based on paleomagnetic inclinations. Before any treatment, the samples were stored in a refrigerated room until processing. The NRM was stepwise AF demagnetized at successive peak fields of 2, 4, 6, 8, 10, 15, 20, 25, 30, 35, 40, 50 m and 60 mT. The analysis of the acquired data followed the same procedures as those applied to borehole RM-CO.

### 4.4 Micropaleontology

Foraminifers serve as valuable biological indicators facilitating the paleoenvironmental characterization of the sediment [Van der Zwaan et al., 1999; Kucera, 2007]. Such micropalaeontological study was particularly useful for defining the coastal depositional environments associated with the successions deposited in the Paleotiber delta between 1.3 and 0.8 Ma [Florindo et al., 2024] and therefore, it was performed.

In this work we present the preliminary data achieved on 17 samples collected from six boreholes: RM-QU, VRE, RM-CO, SA, RM-CA and CAF-S1. From each sample, a 30-60 g fraction was taken, oven-dried, soaked in water, and sieved using mesh sieves with openings > 63 µm and > 125 µm. The resulting fractions (< 63 µm, 63-125 µm, and > 125 µm) were separated by weighing the sieve refuse and expressed as percentage. The analyses were performed on the > 125 µm fraction, but due to the limited number of specimens, only a qualitative analysis was conducted, identifying the main benthic and planktic foraminifer species.

## 5. Results

### 5.1 $^{40}Ar/^{39}Ar$ dating

*TP-CH*

33 sanidine crystals extracted from a bulk sample of Tufo del Palatino pyroclastic-flow deposit yielded a weighted mean age of 528 ± 1 ka (2σ) (Fig. 7a). Other nine crystals yielding ages scattered between 600-800 ka represent xenocrystic contamination from magma of the early Colli Albani activity, as expected for bulk samples of pyroclastic-flow deposits [e.g., Marra et al., 2003; 2020].

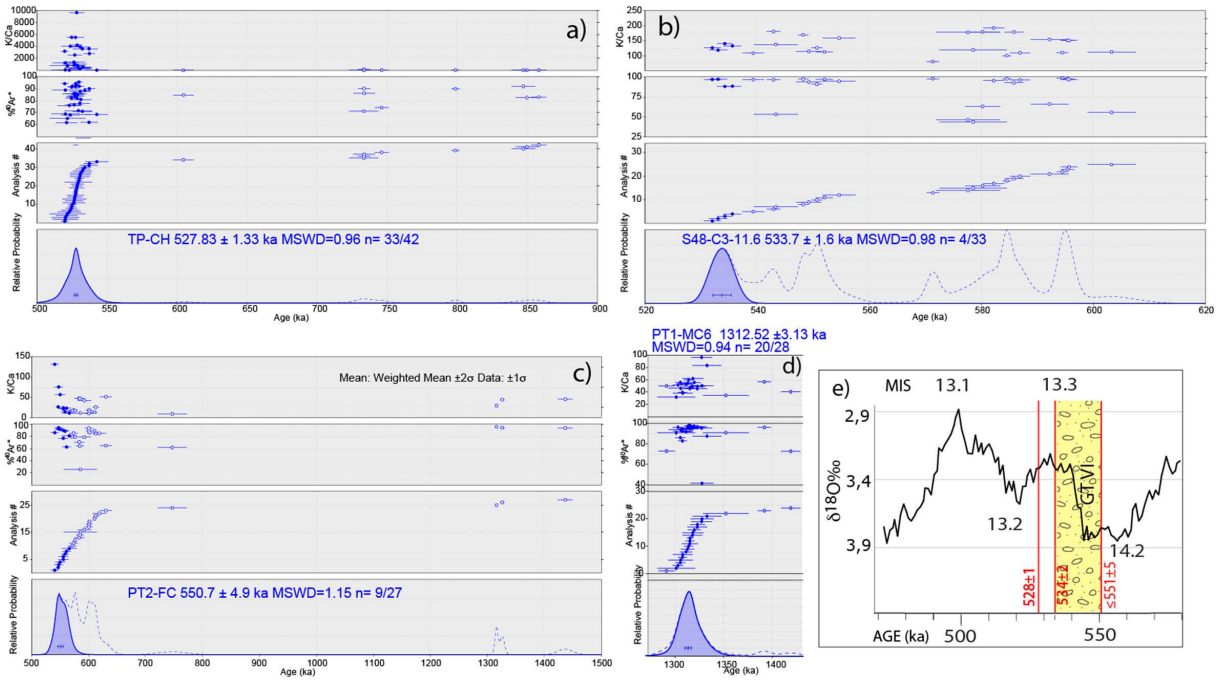


**Figure 7.** a-d) Plots showing age probability and selected control parameters for the dated samples. e) Ages of the dated samples (red vertical bars) are plotted against the astrocalibrated Oxygen Isotope Curve [Lisiecki and Raymo, 2005] to verify the correlation of the aggradational succession with the sea-level oscillations during MIS 13.

Remarkably, this age matches, exactly, the age obtained by Karner et al. [2001a] for a Tufo del Palatino sample from Via Flaminia. However, later re-calibrations of the Fish Canyon Tuff sanidine standard age used for that experiment as well as an update to the $^{40}$Ar decay constant [Min et al., 2000] lead to a re-calculated of the age at 531 ± 2 ka (2σ) [e.g., Marra et al., 2017a]. Note that all of the dates from three Tufo del Palatino sites in Karner et al. [2001a] overlap within uncertainty of our youngest 33 dates from the TdP pyroclastic flow deposit.

*PT2-FC*

A large youngest population of 9 sanidine crystals extracted from the sand matrix in this gravel sample provided a weighted mean age of 551 ± 5 ka (2σ) (Fig. 7b). Such age postdates the end of MIS 15 [563 ka, Lisiecki and Raymo, 2004], excluding that the gravel layer in which the sample was collected might be part of the Paleotiber aggradational succession correlated with MIS 15 (Santa Cecilia Formation) (Fig. 7e).

*S48-C3-11.6*

A youngest population of four crystals in this gravel sample yielded a weighted mean age of 533.7 ± 1.6 hich, in combination with the age of 528 ± 1 ka yielded by the overlying Tufo del Palatino, is a *terminus post-quem* for the glacial termination VI at the onset of MIS 13.3 (Fig. 7e), providing correlation of the dated gravel with the Valle Giulia Formation.

*PT1-MC6*

The largest population of dates from this gravel sample (n = 20) produced a weighted mean age of 1313 ± 3.5 ka (Fig. 7e). One crystal gave a younger date of 1291 ± 16 ka, but it has a much lower radiogenic yield than most of the sanidine analyzed in this sample and therefore likely reflects Ar loss or alteration.

The lack of crystal ages < 1000 ka, also in light of the 960 ka population contained in sample PG1-2, suggests a much older age than the previously hypothesized age within MIS 21 [866-814 ka, Lisiecki and Raymo, 2004] for the Monte Ciocci Formation (Fig. 7f) [e.g. Marra and Florindo, 2014].

## 5.2 Paleomagnetism

*Borehole RM-CO*

Stepwise AF demagnetization enabled isolation of the ChRM component for 10/11 of the samples analyzed (Fig. 8). NRM intensities range from $2.49 \times 10^{-4}$ to $1.32 \times 10^{-2}$ A/m and orthogonal vector diagrams indicate that the magnetization is dominated by a normal component of magnetization. ChRM directions tend toward the origin of the vector component plots, with maximum angular deviation (MAD) values generally < 10°.

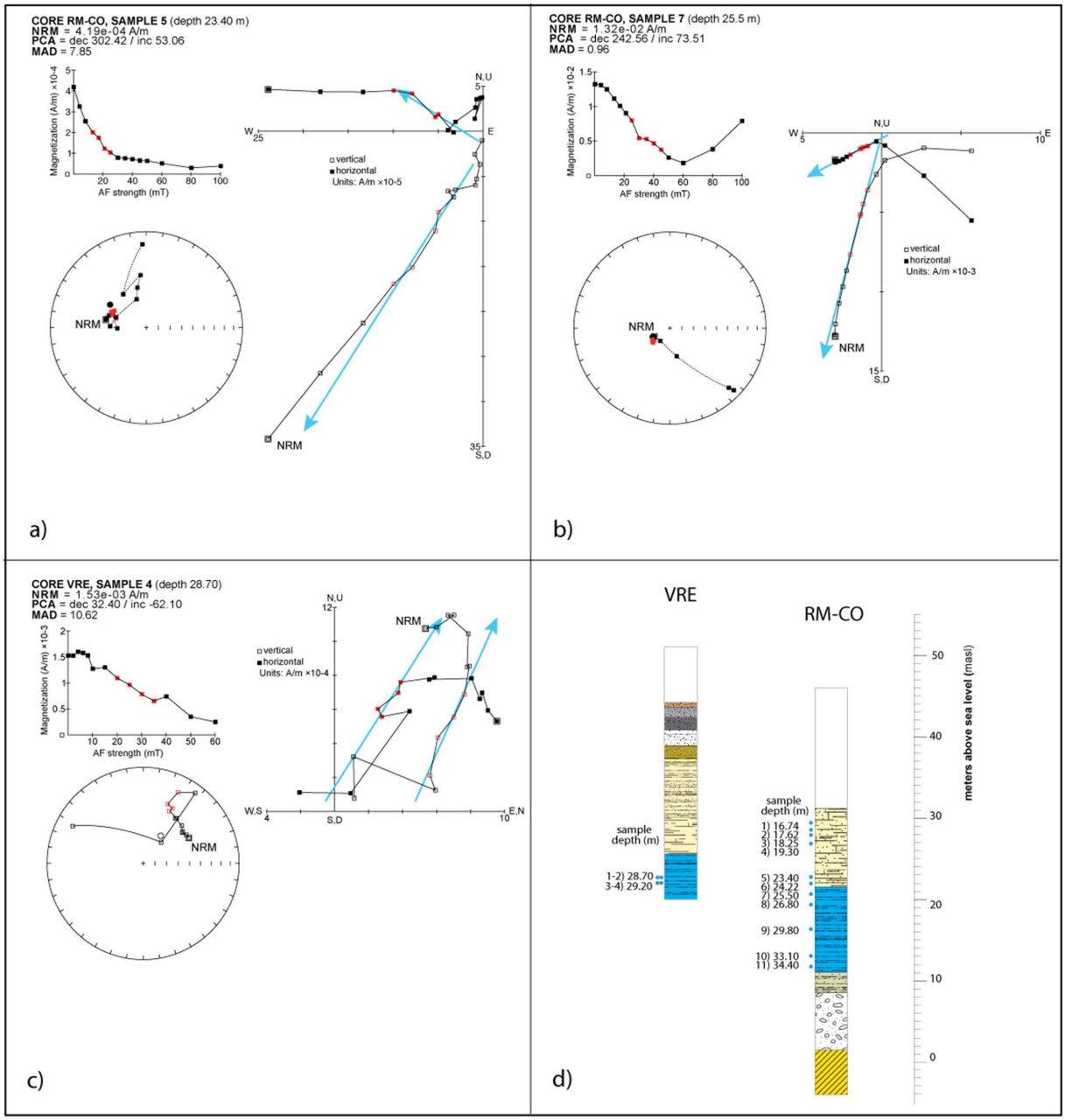


**Figure 8.** a, b) Alternating field demagnetization behavior for two representative samples from core RM-CO; c) Alternating field demagnetization behavior for representative samples from core VRE. For the vector component diagrams, open (closed) symbols represent projections onto the vertical (horizontal) plane. The blue lines represent linear regression fits that indicate the characteristic remanent magnetization (ChRM) direction for each sample. The stereoplots are equal area stereographic projections, where solid (open) symbols represent lower (upper) hemisphere projections. Samples are not azimuthally oriented and declinations are reported in the laboratory coordinate system with respect to the split face of the drill-core; d) Lithology and sampling scheme. PCA = principal component analysis. MAD = maximum angular deviation for the ChRM determination.

*Borehole VRE*

Stepwise AF demagnetization enabled isolation of the ChRM component for 2/4 of the samples analyzed (Fig. 8). NRM intensities range from $5.16 \times 10^{-4}$ to $1.53 \times 10^{-3}$ A/m and orthogonal vector diagrams indicate that the magnetization is dominated by a reverse component of magnetization with MAD values < 10.6°.

## 5.3 Micropaleontological Analyses

*RM-QU Borehole*

Two samples for micropaleontological analyses were retrieved from this core. The foraminifer content of the sample from the oldest depositional yellow clay facies (~2% of sand; RM-QU-25.70) is characterized by a dominance of planktic foraminifers (~70-80%) among which *Globigerinoides obliqus*, *Globorotalia bononiensis*, *Orbulina universa*, *Globigerina bulloides*, *Globorotalia crassaformis*, *Globorotalia inflata* and *Globigerinoides immaturus* are the most abundant. The benthic foraminifer association is also very diverse, and mainly consists of *Planulina ariminensis*, *Cibicides* sp., *Cassidulina carinata*, *Uvigerina peregrina*, *Bulimina elongata*, *Cibicidoides pachyderma*, *Gyroidina soldanii*, *Globobulimina* spp., *Cibicidoides kullenbergi*, *Oridorsalis umbonatus* and *Lenticulina* spp. Following the deposition of a coarse gravel layer, another sandy clay layer was deposited (~23% of sand). Sample RM-QU-18.3 recovered from these facies, was barren in fauna.

*VRE Core*

From the blue clays of this core, only one sample was analyzed for micropaleontological content (VRE-28.9). The latter does not contain very abundant planktic and benthic foraminifers, but the associations are, nonetheless quite diverse. The dominant planktic foraminifer species are *Neogloboquadrina acostaensis*, *G. bulloides* and *Globoturborotalita apertura*, while *Cibicides lobatulus* and *C. carinata* dominate the benthic association. Several other species are additionally present, but significantly less dominant (Table 2).

*RM-CO Borehole*

From the depositional sequence of RM-CO borehole, five samples were analyzed for their micropaleontological content. Sample RM-CO-46.35, taken from the lowermost clay layer (~< 0.5% sand), is characterized by *G. bulloides* and *N. acostaensis* as dominant planktic species, while *G. soldanii*, *C. carinata* and *Cibicides* sp. make up for most of the benthic species' association (Table 2). Some disarticulated ostracod valves were also found. This clay facies is followed by the deposition of a coarse gravel layer, topped by several meters of initially blue and afterwards yellowish clays both with variable sand content. The base of the blue clays (sample RM-CO-34) is barren in microfauna and only some rare bivalve shells fragments could be identified. Moving towards younger layers of the blue clay facies, sample RM-CO-26.9 sand content increased (~15%) and very rare, planktic and benthic foraminifer are present (Table 2) sided by bivalve shells fragments and some ostracods, while by the top of the same facies, all fauna disappears (RM-CO-24). The uppermost sample (RM-CO-18.25), deriving from the predominately yellowish clays facies with ~8% sand fraction, contains, among the dominant planktic foraminifer species *G. apertura*, *N. acostaensis* and *G. bulloides* (Table 2), while *G. crassaformis* is less abundant. The benthic foraminifer association is composed predominately by *C. carinata*, *Globobulimina* spp., *Ammonia parkinsoniana* and *C. lobatulus*, while numerous other species are subordinate (Table 2).

*SA Core*

From this core, two samples were retrieved, one from the grey sandy clays (SA-C5-20), and the other one above, from the yellow clay facies (SA-C5-18). The first one, while rich in sand (~> 55%), contained only a few benthic and planktic badly preserved specimens, while the second one was completely barren (Table 2).

*RM-CA Borehole*

The lowermost sampled facies (RM-CA-39.2), composed of a clay matrix but abundant sand fraction (~> 50%), revealed the presence of planktic and benthic foraminifers as well as fragmented bivalve shells. Among the planktic species, *G. bulloides*, *G. apertura*, *Globorotalia punticulata* and *N. acostaensis* were the most abundant, while *C. lobatulus* and *Cibicides* sp. dominated the benthic association (Table 2). Following a gravel layer, deposition continues with a fining upward predominately clay sequence (from ~11% to ~< 0.5% of sand). The lowermost

sample (RM-CA-34) of this unit shows very diverse associations of both benthic and planktic foraminifers and is also characterized by the presence of few bivalve shells' fragments. Among benthic species, the most abundant are *A. parkinsoniana*, *C. lobatulus*, *C. carinata*, *Valvulineria bradyana*, *Asterigerina planorbis*, *Bulimina aculeata*, *Sphaeroidina bulloides* and *Elphidium crispum*. On the other hand, the dominant planktic species are *G. bulloides* and *G. crassaformis* (Table 2). As sand content decreases, the faunal abundance follows the same trend and wile sample RM-CA-30 still contains some rare benthic and planktic foraminifer specimens, the uppermost sample is completely barren in microfauna (RM-CA-25.5) and only shows some bivalve, gastropod and ostracod shells.

*CAF-S1 Borehole*

Immediately above a coarse gravel facies of core CAF-S1, from the sandy clay layer, sample CAF-S1-44.5 (~8% of sand) was taken and contained a discreetly diverse foraminifer association accompanied by some fragmented bivalve shells. Most abundant among the planktic species were *G. bulloides* and *N. acostaensis*, while the benthic association was composed of *C. carinata*, *A. planorbis*, *C. lobatulus*, *Haynesina germanica*, *Ammonia beccarii* and *A. parkinsoniana*. Subordinate species were also present (Table 2). Two more samples were retrieved from this site (CAF-S1-40 and CAF-S1-35.5). The first one, coming from the middle of the deposit, was barren in fauna and only some bivalve shells fragments and wood particles could be identified. The second one, characterized by an increase in sand content (~21%) contained, in contrast, a diversified, but quite scarce benthic foraminifer association (Table 2).

| Sample | Sand % | Dominant species | Rare species | Other | Environment |
|---|---|---|---|---|---|
| RM-CO-18.25 | 7.77 | **Planktics**: *Globoturborotalita apertura, Neogloboquadrina acostaensis* and *Globigerina bulloides*. **Benthics**: *Cassidulina carinata, Globobulimina* spp., *Ammonia parkinsoniana* and *Cibicides lobatulus*. | **Planktics**: *Globorotalia crassaformis*. **Benthics**: *Ammonia tepida, Brizalina alata, Gyroidina soldani, Bolivina dilatata, Oridorsalis umbonatus, Bulimina striata, Asterigerina planorbis, Cibicidoides kullenbergi, Cibicidoides pachyderma, Melonis pompilioides* and *Rosalina* sp.. | / | Infralittoral environment with river influence |
| RM-CO-24.00 | 0.91 | Barren | Barren | / | Continental |
| RM-CO-26.90 | 15.32 | Very rare foraminifers. | **Planktics**: *Globorotalia scitula, G. bulloides, N. acostaensis, G. crassaformis* and *G. apertura*. **Benthics**: *B. alata, A. planorbis, Cibicides* sp., *Nonion commune, C. lobatulus, Ammonia beccarii, Uvigerina peregrina*, *Pullenia bulloides, G. soldanii* and *C. carinata*. | Some bivalve shells fragments and rare ostracod valves. | Mesolittoral environment, transported fauna |
| RM-CO-34.00 | 1.91 | Barren | Barren | Abundant bivalve shells fragments. | Upper delta plain (supralittoral environment) |
| RM-CO-46.35 | 0.43 | **Planktics**: *G. bulloides* and *N. acostaensis*. **Benthics**: *G. soldanii, Cibicides* sp. and *C. carinata*. | **Planktics**: *Globigerinoides immaturus, Globigerinita glutinata, Turborotalita quinqueloba, Globorotalia inflata, G. crassaformis* and *Orbulina universa*. **Benthics**: *C. lobatulus, P. ariminensis, A. parkinsoniana* and *Eggerella bradyi*. | Some ostracods valves. | Infralittoral to circalittoral environment with river influence |
| RM-CA-25.50 | 0.45 | Barren | Barren | Bivalve and gastropods shell fragments. Some rare ostracod valve. | Alluvial plain or marsh, more freshwater influence. |
| RM-CA-30.00 | 1.78 | Barren | Extremely rare benthic and planktic foraminifer fragments. | Bivalve shells fragments. | Coastal plain, with some transported individuals |

| Sample | Sand % | Dominant species | Rare species | Other | Environment |
|---|---|---|---|---|---|
| RM-CA-34.00 | 11.38 | **Planktics**: *G. crassaformis* and *G. bulloides*. **Benthics**: *A. parkinsoniana, C. lobatulus, C. carinata, Valvulineria bradyana, A. planorbis, Bulimina aculeata, Sphaeroidina bulloides* and *Elphidium crispum*. | **Planktics**: *G. apertura, Globoturborotalita woodi, N. acostaensis* and *O. universa*. **Benthics**: *G.a soldanii, Cibicidoides bradyi, Melonis barleeanus, P. ariminensis, C. pachyderma, Globocassidulina subglobosa, N. commune, Bolivina antiqua, Bulimina elongata* and *U. peregrina*. | / | Infralittoral to upper circalittoral environment rich in organic matter |
| RM-CA-39.20 | 50.65 | **Planktics**: *G. bulloides, G. apertura, Globorotalia punticulata* and *N. acostaensis*. **Benthics**: *C. lobatulus* and *Cibicides* sp.. | **Planktics**: *G. glutinata* and *Globigerina decoraperta*. **Benthics**: *G. soldanii, E. crispum, Bolivina spathulata* and *U. peregrina*. | Very rare bivalve shells fragments. | Mesolittoral environment with transported fauna |
| RM-QU-18.30 | 22.81 | Barren | Barren | Barren | Continental |
| RM-QU-25.70 | 2.07 | **Planktics**: *Globigerinoides obliqus, Globorotalia bononiensis, O. universa, G. bulloides, G. crassaformis, Globorotalia inflata* and *Globigerinoides immaturus*. **Benthic**: *P. ariminensis, Cibicides* sp., *C. carinata, U. peregrina, B. elongata, C. pachyderma, G. soldanii, Globobulimina* spp., *Cibicidoides kullenbergi, O. umbonatus* and *Lenticulina* spp.. | **Planktics**: *Globigerinoides sacculifer, Globoturborotalita decoraperta, N. acostaensis* and *G. scitula*. **Benthics**: *Bolivina reticulata, Cancris auricula, G. subglobosa, M. barleeanus, Brizalina arta, Pleurostomella alternans, Amphycorina* spp., *C. bradyi, Karreriella bradyi* and *Sphaeroidina bulloides*. | / | Epibathyal to mesobathyal environment |
| SA-C5-18.00 | higliy cemented clay | Barren | Barren | / | Continental |
| SA-C5-20.00 | 55.46 | Barren | Very rare benthic foraminifer transported, badly preserved specimens. | / | Emerged beach |
| CAF-S1-35.50 | 21.24 | Very rare foraminifers. | **Planktic**: *G. bulloides, G. glutinata, G. crassaformis, N. acostaensis* and *G. decoraperta*. **Benthics**: *A. planorbis, A. beccarii, B. aculeata, G. soldanii, V. bradyana, B. arta, M. pompilioides, U. peregrina, N. commune, G. subglobosa, C. lobatulus, A. parkinsoniana, Lagena* spp. *Cibicides* sp. and *Lenticulina* spp.. | / | Mesolittoral environment with transported fauna |
| CAF-S1-40.00 | 2.40 | Barren | Barren | Some bivalve shell fragments and abunandt wood. | Alluvial plain or marsh, more freshwater influence. |
| CAF-S1-44.50 | 7.85 | **Planktics**: *G. bulloides* and *N. acostaensis*. **Benthics**: *C. carinata, A. planorbis, C.s lobatulus, Haynesina germanica, A. beccarii* and *A. parkinsoniana*. | **Planktics**: *G. glutinata, G. crassiformis, T. quinqueloba* and *G. decoraperta*. **Benthics**: *G. soldani, M.s pompilioides, B. dilatata, C. kullenbergi* and *S. bulloides*. | Rare bivalve shells fragments. | Infralittoral with river influence |
| VRE-28.90 | 23.89 | **Planktics**: *N. acostaensis, G. bulloides* and *G. apertura*. **Benthics**: *C. lobatulus* and *C. carinata*. | **Planktics**: *O. universa, G. glutinata, G. scitula, G. obliqus* and *G. crassiformis*. **Benthics**: *Cibicides* sp., *M. pompilioides, B. aculeata, N. commune, Lagena* sp., *P. bulloides, A. parkinsoniana, Bucella granulata, E. crispum, G. soldani* and *A. planorbis*. | / | Transition between and infralittoral and circalittoral environment |

**Table 2.** Summary of micropaleontological data.

## 5.4 Borehole's Stratigraphy

Detailed sedimentologic description of the investigated boreholes is reported in Suppl. Mat. #1. A summary of their stratigraphy is provided in Figure 9.

*Borehole RM-QU*

A 16.5 m thick cover of anthropic fill was encountered by this borehole above a fluvial-lacustrine sedimentary succession erosionally overlying the Pliocene marine clay substrate, reached at 19.90 m asl (Fig. 9 and S1). Micropaleontological analysis on sample RM-QU-25.7 revealed the occurrence of the association of *G. bononiensis, G. crassaformis and G. inflata* [MPL5b Interval subzone, Lirer, 2019], which is characteristic of the basal portion of the Gelasian-Calabrian ingressive cycle in the Rome's area [Marra et al., 1995; Bulian et al., 2024]. The overlying "Paleotiber" succession is composed of a basal coarse gravel horizon, 4.10 m thick. The gravel passes abruptly upward to coarse sand in scarce yellow silty matrix, 2.60 m thick, which includes a 15 cm thick pedogenic layer, dark brown in color, suggestive of temporary exposure. A 40 cm thick yellow sandy silt layer overlies this sand horizon and is followed by another, only 30 cm thick coarse gravel layer. The micropaleontologic analysis on one sample of the silt shows that it is barren. The two sand and clay layers are interpreted as a lens of fine-grained fluvial sediment within the basal gravel layer of the aggradational succession. Therefore, the top of the gravel horizon, considered as a whole, occurs at 27.30 m asl, consistent with borehole data showing elevation around 28 m asl for this lithologic boundary in this sector. The 1.20 m thick coarse sand deposit cored above 27.30 m is in turn the lower part of the fine-grained portion of the aggradational succession.

Three vertically oriented samples collected in the 40 cm-thick silt layer interbedded in the upper part of the gravel horizon yielded a week paleomagnetic signal, hindering any chronological consideration.

*Borehole RM-CO*

No volcanic deposit was encountered in this borehole, recovering 15 m of anthropic fill (including an 8 m tall Roman age masonry structure) directly overlying the typical "Paleotiber" aggradational succession described in central Rome by Marra and Rosa [1995] (Fig. 9 and S1). This is represented, from top to bottom, by 9.4 m of yellow sandy clay with thin travertine layers ("Paleotiber Unit 2b") conformably overlying (a gradual lithologic transition has been observed) a 10.4 m package of homogeneous grey clay with rare organic veils; this transitions to a 2.9 m thick horizon of sandy clay with oxidation veils a sparse fine gravel at the base, abruptly passing downward to a 6.9 m thick layer of coarse gravel ($ø \leq 10$ cm) in light brown silty sand matrix ("Paleotiber 2a Unit"). The top of the gravel layer occurs at 8.4 m asl, while the top of the Pliocene substrate is found at 1.5 m asl.

Eleven vertically oriented samples collected throughout the Paleotiber succession in the yellow sandy clay and the grey clay yielded normal paleomagnetic polarity. This paleomagnetic constraint provides a terminus post-quem of 773 ka [Matuyama-Brunhes reversal, Singer, 2014] to their deposition, disproving previous attribution to MIS 19 for the Paleotiber succession occurring in this sector of Rome [Paleotiber 2 Unit, Marra and Florindo, 2014].

The micropaleontological analysis on sample RM-CO-46.35 (Table 2) allows to attribute the marine substrate to the late Pliocene due to the compresence of *G. crassaformis* and *G. inflata* [Marra et al., 1995; Bulian et al., 2024]. The "Paleotiber" succession above the basal gravel horizon is characterized by a transitional continental-to marine environment (supralittoral), like an upper delta plain with high freshwater influence (samples RM-CO-34, RM-CO-26.9, Table 2). Moreover, after a temporary emergence testified by the complete lack of fauna in the yellow clay sample RM-CO-24, a marked shift towards more open marine conditions (infralittoral) occurs in the uppermost part of the succession (sample RM-CO-18.25, Table 2).

*Borehole RM-CA*

Also, this borehole missed the volcanic cover, recovering the fluvial-lacustrine deposits of two distinct, $< 600$ ka aggradational successions below 8 m of anthropic fill (Fig. 9 and S1, S2). The occurrence of idiosyncratic orange tuff fragments of Tufo Lionato ($365 \pm 4$ ka) within the sandy silt deposits cored between 8.15-9.25 m depth, facilitate their attribution to the MIS 9 aggradational succession [Aurelia Formation, Conato et al., 1980; Marra and Rosa, 1995; Karner and Marra, 1998], although a less probable correlation with the younger Vitinia Formation [MIS 7, Conato et al., 1980; Marra and Rosa, 1995; Karner and Marra, 1998] cannot be excluded.

A marked erosive contact separates this succession from the underlying yellowish, compact sandy silt, passing downwards to bedded yellow silty sand with frequent intercalations of reworked volcaniclastic layers and primary

fallout layers. The gray granular (lapilli-sized) as well as greenish fine ash features of the volcanic intercalations strongly suggest their origin from the reworking of the Colli Albani and Monti Sabatini volcanic deposits erupted in the 561-516 ka interval, providing correlation with the MIS 13 aggradational succession [Valle Giulia Formation, Marra and Rosa, 1995; Karner and Marra, 1998; Marra et al., 2017a] (see Fig. 10). A detailed description of this portion of the borecore is provided in Figure S2. Another sharp erosive contact separates the MIS 13 fluvial-lacustrine deposits from the underlying 12 m thick package of homogeneous grey clay with rare organic veils and scarce sand fraction in the lowest 2 meters. A 50 cm thick sand horizon marks the abrupt passage to a medium-coarse gravel layer (ø ≤ 6 cm) in whitish silty-sand matrix, 1.8 m thick. The top of the gravel layer is at 2.0 m asl, while the top of the Pliocene substrate is at 0.2 m asl. The latter is here represented by older deposits of the *G. puncticulata* biozone (sample RM-CA-39.2, Table 2).

The lower part of the "Paleotiber" succession in this borehole displays frank marine characters (infra- to upper circa-littoral environment, sample RM-CA-34), and progressively transition upwards to a meso-littoral (coastal plain, sample RM-CA.30, Table 2) and to a fluvial-dominated (alluvial plain, sample RM-CA-25.5) environment.

*Borehole CAF-S1*

The complete typical Colli Albani and Monti Sabatini volcanic succession emplaced in the area of Rome [Marra and Rosa, 1995; Karner et al., 2001a] has been observed in the cores of this borehole supported by Fondazione Amici di Italia Fenice as part of a Geological Monograph Project on Caffarella and with the permission and field support of the Ente Regionale Parco dell'Appia antica and of the Parco Archeologico dell'Appia antica (see Fig. 9 and, for detail, S3). The primary volcanic deposits include, from top to bottom, Pozzolanelle/Tufo Lionato, Pozzolane Nere, Pozzolane Rosse, Earthy Tuffs with White Pumice, Grottarossa Pyroclastic Sequence, Tufo Giallo di Prima Porta, Tufo del Palatino, Tufo Giallo della Via Tiberina (sub-primary), and Tufo Pisolitico di Trigoria. A ca. 2 m thick characteristic volcaniclastic horizon ("Conglomerato Giallo"), equivalent of the MIS 11 San Paolo Formation [Marra and Rosa, 1995; Karner and Marra, 1998], has been recovered at the top of the Pozzolane Rosse pyroclastic-flow deposit. A 4.2 m thick sedimentary succession constituted by whitish carbonatic silts intercalated with grey and yellowish sandy clay and including a 60 cm thick, greenish volcaniclastic sand layer, underlies the Tufo Pisolitico di Trigoria. It displays erosive contact, marked by a 1 cm-thick organic (sapropel-like) layer, above a 10.3 m thick package of homogeneous grey clay with organic veils, passing abruptly to a 4 m thick horizon of coarse gravel (ø ≤ 10 cm) in light brown sand matrix. The top of the gravel layer occurs at 1.2 m asl, while the top of the Pliocene substrate [*G. puncticulata* biozone, from a sample collected ad 49.5 depth analyzed in Bulian et al., 2024] is found at -2.8 m asl.

The "paleotiber" succession above the basal gravel layer displays very similar features as that encountered in borehole RM-CA, consistent with the same elevation and the common paleogeographic, southern location of these boreholes (Fig. 9). The blue clays are characterized by an infralittoral to circalittoral environment under river influence (sample CAF-S1-44.5, Table 2), which after a temporary shift into a marsh or alluvial plain where the marine influence is minimal (sample CAF-S1-40), transitions upwards to a mesolittoral environment (sample CAF-S1-35.5).

*Boreholes SA, S43, S48*

Several cores from a drilling campaign performed at the Capitoline Hill in the 90's, the stratigraphic logs of which were published in Alvarez et al. [1996], have been re-examined and sampled by concession of the Soprintendenza Capitolina. The cores of three boreholes (S43, S48, SA, Fig. 9) allowed us at reconstructing a composite section between 28 and 4 m asl, including the Tufo del Palatino pyroclastic-flow deposit and the underlying aggradational succession resting above the Pliocene substrate. This section has been merged with the larger cross-section reconstructed through the analysis of all the available stratigraphic logs and outcrop data by D'Ambrosio et al. [2023] (Fig. 9).

The stratigraphic setting at the Capitoline Hill provides a summary of the factors underlying to the interplay among glacio-eustatic oscillations, volcanic activity, tectonics, and sedimentation. Three aggradational successions correlating with MIS 13, MIS 11 and MIS 9, characterized by unconformable contacts along deep erosional incisions, are exposed along the flanks of the hill: Valle Giulia, San Paolo, and Aurelia Formations (Fig. 9). The pyroclastic-flow deposits of Tufo del Palatino (TdP) and Tufo Lionato are embedded at the base of the Valle Giulia and Aurelia Formations, respectively, while the Tufo Giallo di Prima Porta directly overlies the TdP where the latter is emplaced on a morphological height. The base of the TdP flow displays indeed a variable elevation, as a result of the infilling of a paleoincision, possibly originated by combined effect of the MIS 14 sea-level lowstand and fault displacement [e.g., Rosa, 2022], cutting through the underlying Paleotiber aggradational succession and resting on top of the

gravel horizon at the bottom of the paleoincision. A gravel sample collected within the gravel layer (S48-C3-11.6), dated in the present study, yielded a maximum age of 533.7 ± 1.6 ka, confirming attribution of the aggradational succession to the Valle Giulia Formation [D'Ambrosio et al., 2024]. The micropaleontologic analysis on the grey sandy silt and the yellow sandy clay recovered in borecore SA suggest an emerged coastal environment (as provided by rare badly preserved benthic foraminifers in sample SA-C5-20), followed by a complete continentalization of the environment, as the yellow facies does not contain any fossils (sample SA-C5-18).

*Lapis Niger Outcrop*

An archaeological excavation at the *Lapis Niger* in the Roman Forum exposed a gravel bank in a sandy matrix partially cemented towards the bottom, with calcareous and siliceous pebbles of 8-10 cm maximum diameter, in which one sample for detrital sanidine dating was collected (PT2-FC). This bank, with an eroded upper surface, constitutes the substratum of the archaeologically frequented layers containing, among other things, an ancient spring, a votive *favissa*, the structure of the *Comitium* (royal age-republican age) and the *Lapis Niger*, with variable overall thicknesses between approximately 2 and 4 meters starting from the flooring of the Roman Forum in the imperial age, which is located approximately 13.36 meters above sea level. Despite the elevation of the sampled gravel (ca. 9 m asl) matches that of the wide basal gravel horizon of the Paleotiber succession in this sector (Fig. 9), the maximum age of 551 ± 5 ka yielded by sample PT2-FC, combined with that of 534 ± 2 ka yielded by the other sample collected in the same gravel layer, exclude correlation with MIS 15 or older. In contrast, these ages provide correlation with glacial termination VI at the onset of MIS 13 (see Fig. 7f). Therefore, the aggradational succession comprised at least between 6 m and 20 m asl at the Capitoline Hill is attributed to the Valle Giulia Formation, consistent with the reconstruction of the stratigraphy in D'Ambrosio et al. [2023]. It cannot be excluded, however, that the lowest portion of the gravel belongs to an older aggradational succession which correlates with the Paleotiber succession occurring in central Rome. Also consistent with the stratigraphic setting of the Valle Giulia Formation highlighted at Viale Flaminio in Marra et al. [2017], the Tufo del Palatino displays erosive features filling a paleo-valley incised in the early MIS 13.3 aggradational succession [Fig. 9, D'Ambrosio et al., 2024].

*Borehole VRE*

A 50 cm-long core was collected in the grey clay horizon of the Paleotiber succession encountered by several boreholes drilled for civil engineering purpose at the Peroni brewery plant in Via Reggio Emilia (VRE in Fig. 9).

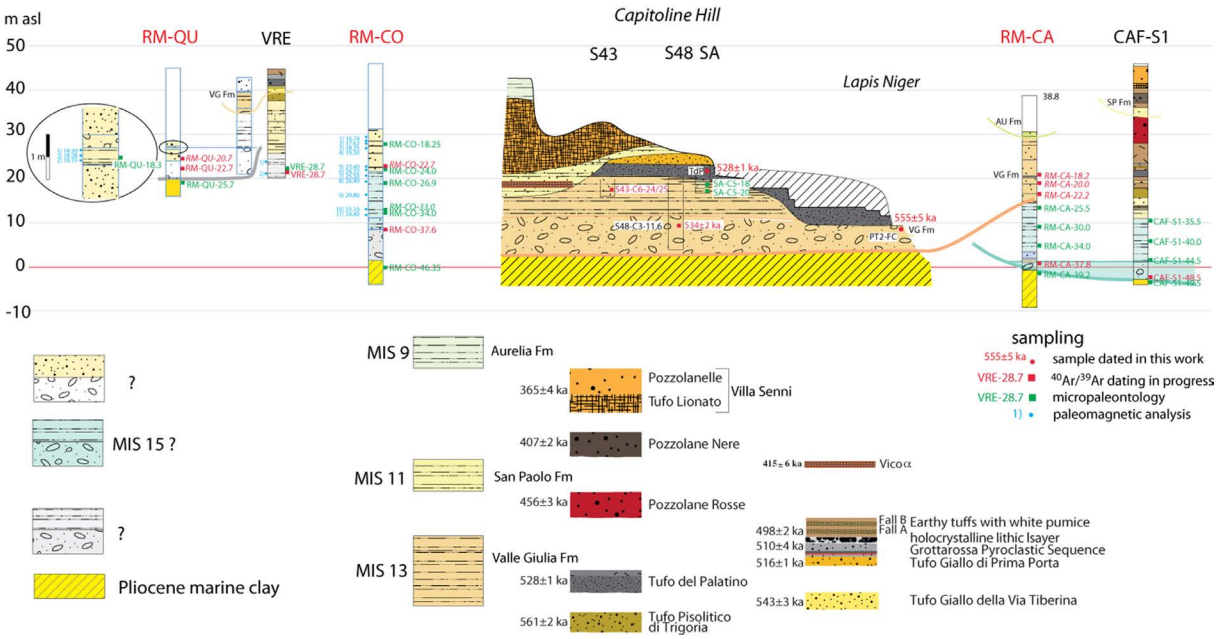


**Figure 9.** Preliminary correlation among the dataset of boreholes performed by INGV (red label) and those observed in the present work, showing position of the collected samples. See Figure 5 for location.

Paleomagnetic analysis on four vertically oriented samples collected in this core showed their reversed polarity, evidencing their older age (pre- Matuyama-Brunhes) with respect to the "Paleotiber" succession recovered in borehole RM-CO. In contrast, the paleomagnetic analysis confirms the correlation with the clay section previously investigated by Florindo et al. [2007] in borehole PSA, which was attributed to MIS 19. However, stratigraphic considerations based on new borehole log data examined in the present work suggest an even older age for these "Paleotiber" successions (see section 6.1.1).

The micropaleontologic analysis on sample VRE suggests a marine transitional environment, between infra-littoral and circa-littoral.

# 6. Discussion

## 6.1 Chrono-Stratigraphic Setting

### 6.1.1 "Paleotiber" Successions

These successions constitute the first continental deposit above the Plio-Pleistocene marine substrate in central Rome and are always represented by a basal horizon of gravels, several meters thick. However, the stratigraphic relationships among the gravel layers of different aggradational successions in the interval encompassing MIS 19 through MIS 15 (800-600 ka) are not easily determinable for these buried sedimentary horizons, due to the lack of marked elevation gain in this sector, the erosive nature of the contacts and the discontinuous borehole stratigraphic evidence.

In particular, two similar aggradational successions constituted by a basal gravel horizon, 6 to 10 m thick, passing upwards to a several m-thick package of grey clay followed by yellow clayey sand have been distinguished and correlated with MIS 19 and MIS 15, based on coupled $^{40}Ar/^{39}Ar$ and paleomagnetic age constraints, despite the apparent lateral stratigraphic continuity [Florindo et al., 2007; Marra and Florindo, 2014]. In contrast, no aggradational succession confidently attributable to MIS 17 has been recognized so far in central Rome.

However, the new paleomagnetic analysis in core RM-CO revealing that the overall clay section above the basal gravel horizon has normal polarity imposes a revision of the previous attribution to MIS 19 of the Paleotiber succession in central Rome, suggesting possible correlation with MIS 15 or MIS 17. Both hypotheses are consistent with the micropaleontological evidence from RM-CO, showing the occurrence of two successive marine ingressions corresponding to the lowest and uppermost fine-grained portions of the aggradational succession. Indeed, each one of these isotopic stages is characterized by two consecutive sea-level oscillations, corresponding to as many isotopic peaks: MIS 15.5/15.1 and MIS 18.3/17.1, respectively. However, the most conservative alternative hypothesis is that the aggradational succession recovered in RM-CO correlates with MIS 15 and is the same cycle occurring in the southern sector of the Rome's area. However, the distinction between two diachronic aggradational successions is suggested by the attitude of the basal gravel horizons, which have very homogeneous elevations around 0 m in the sector south of Caracalla Baths, and around 10 m a.s.l. between Caracalla Baths and RM-CO (Figs. 10 and 11a). Detrital sanidine dating in progress may help to clarify this issue.

More complicated appears the stratigraphic relationship between RM-CO and the northern sector where the boreholes in which the clay sections have yielded reversed polarity occur (VRE and PSA boreholes). In particular, ten boreholes (including VRE) drilled at the ancient Peroni brewery plant have allowed to recognize the occurrence of multiple gravel layers at different elevation in this sector (see cross-section B-B′ in Fig. 10). Combined with the age $< 1313 \pm 4$ ka obtained for the Monte Ciocci gravel layer, the occurrence of such multiple gravel layers suggests that a progressive, sin-sedimentary tectonic dislocation affected the early aggradational successions deposited in the Paleotiber delta 1.3 through 0.8 Ma, as shown in the cross-section B-B′ of Figure 9. When the older age for these gravel layers is considered, also the attribution to MIS 19 of the aggradational succession recovered in borehole PSA may be questioned. The lateral correlation among the different boreholes investigated in the northern area of Rome according to the interpretation by Florindo et al. [2007] is reported in cross-section A-A′ of Figure 10, where one single aggradational succession correlating with MIS 19 is recognized. Indeed, the interval yielding normal polarity in the middle of the grey clay section occurring in PSA was interpreted as deriving from later re-magnetization due to the diffuse presence of iron sulphides [i.e., "Greigite"; Florindo et al., 2007]. However, the paleomagnetic signal in such interval may be, at least in part, pristine, suggesting an alternative correlation either with MIS 21

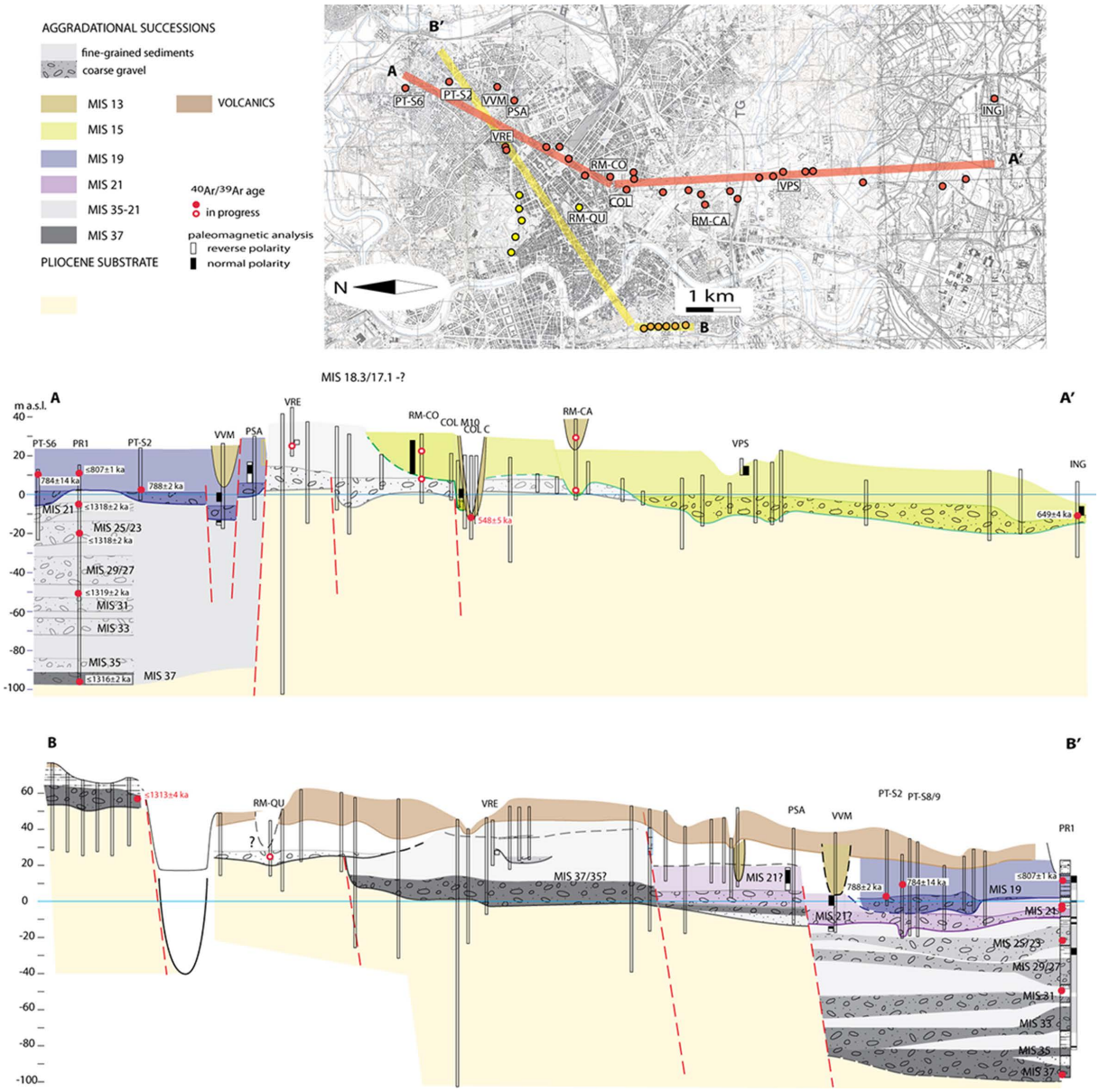


**Figure 10.** Reconstruction of the lateral correlation among the Paleotiber aggradational successions in the greater area of Rome achieved thorough the interpretation of observed borecores (with label) and selected archive stratigraphic logs. Two alternative interpretations for the correlation of the aggradational successions occurring within the Paleotiber graben are reported in cross-section A-A′ [according to Florindo et al., 2007], and in cross-section B-B′ (this work).

or MIS 25 (cross-section B-B′ in Fig. 10), as provided by the paleomagnetic signal of the clay sections analyzed in borehole PR1 by Florindo et al. [2024].

A tentative reconstruction of the complex stratigraphic relationships among the different aggradational successions occurring in the historical center of Rome is provided in the present work, thanks to the analysis of the stratigraphic logs of the boreholes drilled in the years 1998-2011 for the realization of the subway Metro C. Their integration with those stored in the INGV database and with some crucial direct observations, allowed to reconstruct an abandoned channel of the Paleotiber, between the Capitoline Hill and the Colosseum, in which the three aggradational successions correlated with MIS 15, MIS 13, and MIS 11 are embedded with each other (Fig. 11). In particular, the basal gravel layer of a channeled MIS 15 aggradational succession, characterized by a distinctive section of “blue clays” (i.e., homogeneous grey clay with diffused veils of organic matter), which does not occur in later fluvial-dominated aggradational successions displaying coarser grainsize and yellow to light brown color, can

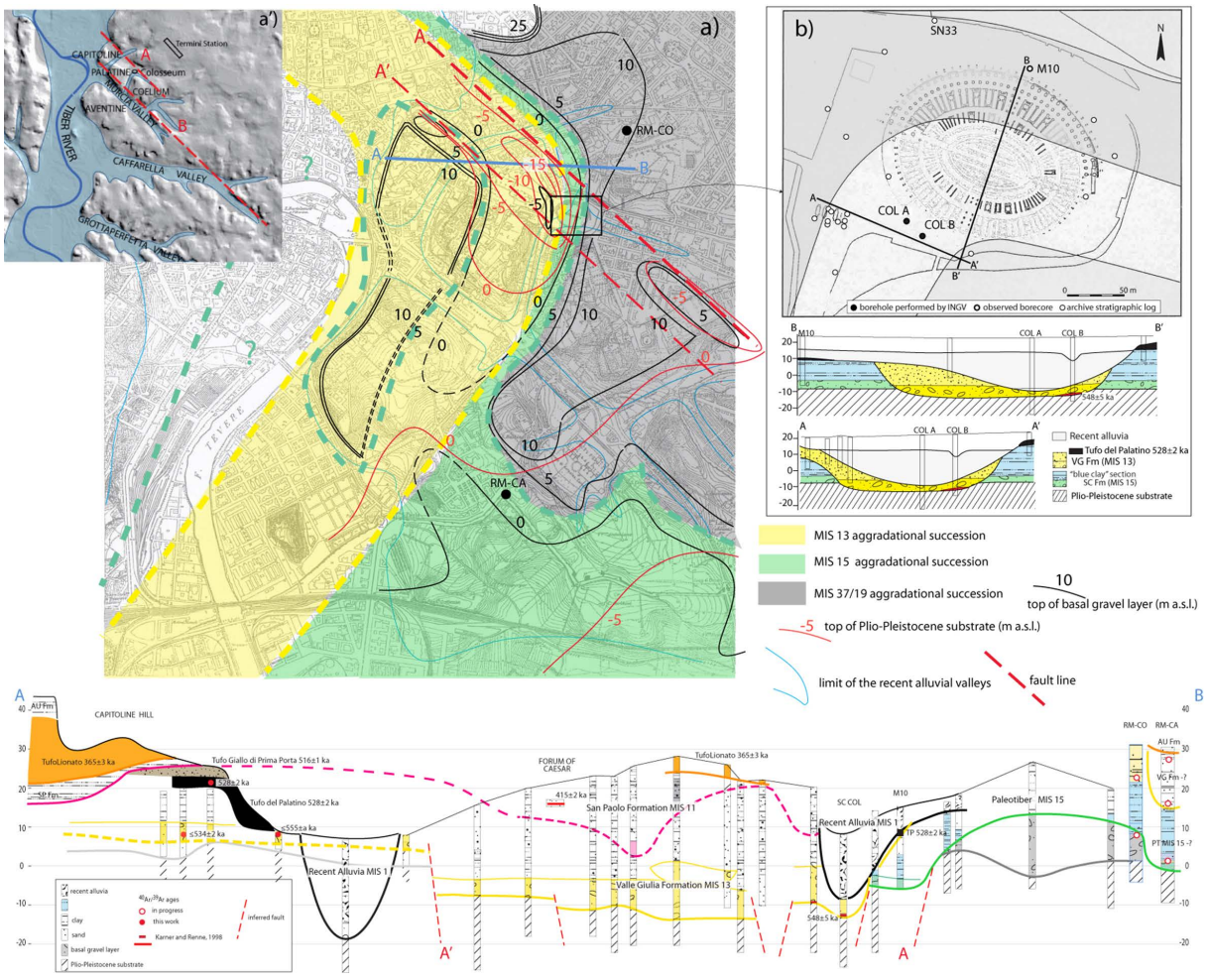


**Figure 11.** a) The integration of the analyzed Metro C boreholes with those stored in the INGV database and with direct borecore observation, allowed to reconstruct the geometry of the gravel layers, highlighting an abandoned channel of the Paleotiber, between the Capitoline Hill and the Colosseum. The complex pattern of embedded aggradational successions is shown the in cross-section. Comparison of the trend of the top of the gravel layers and of the Plio-Pleistocene substrate evidences a lowered sector which is interpreted as the result of tectonic displacement. The morphologic evidence of the fault responsible for the dislocation (A) is shown in the DEM in inset a′, along with the fault line (B) identified in Marra et al. [2018, 2021] as responsible for the diversion of the Tiber course during the 6th century BCE. b) Geologic map and subsurface geology in the Colosseum area, showing the chronostratigraphic constraints allowing the attribution to the Valle Giulia Formation for the aggradational succession occurring in this sector [modified from Bozzano et al., 1995]. See text for further comments and explanation.

be tracked through the Colosseum and borehole RM-CA, at elevation close to the present sea-level, consistent with the reconstruction made by Marra and Florindo [2014].

Age determinations through detrital sanidine method on sedimentary samples collected at several boreholes are in progress, which may help to dissipate the extant doubts and delineate a more detailed picture of the stratigraphic relationships among these aggradational successions, as also discussed in the next section.

### 6.1.2 "Fluvial-Lacustrine" Successions

The identification and correlation of the "Fluvial-lacustrine" successions (MIS 13 to MIS 7 aggradational successions) encountered in borehole is a challenging task, due to very complex stratigraphic relationships, characterized by superimposed cut-and-fill geometry, and to the scarcity of objective criteria upon which to base their dating.

A discriminating factor in order to unveil this complicated pattern in the historical center of Rome has resulted the direct observation by the authors of the present work of the cores of two boreholes drilled at the Colosseum (COL M10, COL C, Fig. 11). In particular, two boreholes were sponsored and drilled in front of the southwestern arcade of the Colosseum by the INGV in the year 1994, aimed at reconstructing the depth and the borders of the recent alluvial valley crossing through the amphitheater (Fig. 11b) [Bozzano et al., 1995]. These boreholes crossed a peculiar gravel horizon, more than 7 meters thick, occurring between −5.6 and −13.3 m a.s.l. below the erosive surface at the bottom of the recent alluvial deposits. Unlike the gravel horizons occurring at the base of the typical Paleotiber aggradational successions, which is made up of well rounded limestone pebbles, up to 10 cm in diameter, and subordinated rounded chert pebbles, in abundant, whitish loamy sand matrix, the gravel cored in these boreholes was made up almost entirely of sub-angular, medium-sized (ø ≤ 5 cm) chert pebbles, in scarce yellow sand matrix. The absence of carbonate pebbles, not explainable when considering that the main source of gravel in the Tiber catchment is the Meso-Caenozoic carbonate platform of Latium and Abruzzi [Parotto and Praturlon, 1975], can be explained by leaching due to hydrothermal fluids. The occurrence of strong chemical degradation is also supported by the observation of alteration rims affecting the chert pebbles. Indeed, fluid circulation linked with the presence of a NW-SE trending fault is readily associated with the reconstruction of the geometry of the gravel layers in this sector, provided by a large number of boreholes drilled for the realization of the Metro C underground. The top of a lowest gravel horizon occurs at elevation around the present sea level (green shaded area), as opposed to an upper gravel horizon with top around 10 m asl (blue shaded area in Fig. 11). In the southern sector (borehole RM-CM near the Caracalla Baths) elevation of the lower gravel layer matches that of the aggradational succession which has been geochronologically and paleomagnetically correlated with MIS 15 throughout south Rome, from the Colosseum to the ING borehole [Marra and Florindo, 2014] (cross-section A-A′ in Fig. 9). In contrast, within a NW-SE elongated, northern sector the lower gravel layer is tightly constrained within the sea-level rise at the onset of MIS 13 by the $^{40}Ar/^{39}Ar$ age of 548 ± 5 ka [Karner and Renne, 1998] yielded by a pyroclastic-flow deposit occurring at its base in borehole COL-B (Fig. 11b). This is a grey, laminated ash-lapilli deposit which as been recovered in identical stratigraphic position in a Metro C borehole drilled 100 m to the north, displaying the characteristic textural and composition features of the distal Monti Sabatini pyroclastic-flows channeled within the (paleo) Tiber Valley [e.g., Tufo Giallo di Prima Porta, Marra et al., 2017a]. Indeed, its age matches that of the Tufo Giallo della Tiberina [546 ± 3 ka, Marra et al., 2014], allowing a safe correlation.

While the gravel layer below the Colosseum was originally attributed to the Valle Giulia Formation [Bozzano et al., 1995], later works have interpreted the sedimentary succession filling the paleovalley as hosting the MIS 11 aggradational succession [Moscatelli et al., 2012; Pagliaroli et al., 2013; Mancini et al., 2014, 2023, and ref. therein]. However, the $^{40}Ar/^{39}Ar$ ages provided in the present work, combined with the correlation od the Metro C borehole and those performed by INGV confirm previous attribution to MIS 13.

At the southern end of this rectangular sector, the top of the MIS 13 gravel layer drop to -5 m asl. When the strongly anomalous low elevation of the top of the Plio-Pleistocene substrate underlying the MIS 13 gravel in this area is considered, which is more than 15 m lower than the average elevation displayed throughout the surrounding area (Fig. 10), a persistent structural control on the Paleotiber channel, causing significant tectonic subsidence in this area is evidenced. Such tectonic control is the result of a NW-SE trending normal fault (A in Fig. 11a′), consistent with the extensional regime acting on the Tyrrhenian Sea Margin throughout the Pleistocene [Montone and Mariucci, 2016], the geomorphological evidence of which is clearly visible on the Digital Elevation Model. Remarkably, such fault is associated with an even more evident, parallel structural lineament, controlling the geometry of the catchment basins of the Murcia and Caffarella Valleys, to which the fault responsible for the diversion of the Tiber course and the origin of the Tiber Island during the 6th century BCE is associated [B in Fig. 11a′; Marra et al., 2018, 2021b].

The complex pattern of embedded aggradational successions filling the paleo-incisions excavated during periods of sea-level falls 650 through 350 ka is tentatively reconstructed in cross-section of Figure 10′, based on available boreholes stratigraphy and geochronologic constraints. Fluvial-lacustrine deposits of the MIS 11 aggradational succession (San Paolo Formation), testified by the outcrop at the Forum of Caesar where a pumice fallout layer embedded within silty sands was dated at 416 ± 8 ka [Karner and Renne, 1998] (= Vico α eruption unit, 415 ± 2 ka; Pereira et al., 2020), overlay with an erosional contact the deposits of the MIS 13 Valle Giulia Formation. However, the contact between these aggradational cycle is only tentatively assessed (dashed magenta line in Fig. 11), based on the occurrence of a possible basal gavel layer of the San Paolo Formation. Notably, the relatively poorly marked erosional contact and the complete burial of the deposits of the Valle Giulia Formation by those of the San Paolo

Formation reflects the significantly higher maximum sea level reached during MIS 11c highstand, 6-13 m above present, which is explained as due to a ~15 kyr-long episode of intense poleward heat flux transport 425 through 410 ka [Hu et al., 2024].

More evident is the erosional surface correlating with MIS 10 sea-level fall (orange line in), as it is overlain by the Tufo Lionato pyroclastic-flow deposit (365 ± 3 ka). The latter is partially eroded during the glacial maximum and successively overlaid by the fluvial-lacustrine deposits of the MIS 9 aggradational succession (Aurelia Formation). These are distinguished from the similar deposits of the successive Vitinia Formation (MIS 7) at the Capitoline Hill, where they are dated at 352 ± 2 ka at the Rupe Tarpea, as opposed to the sedimentary succession overlying the Tufo Lionato on the Aventine Hill, which is correlated with MIS 7 by the maximum age of 278 ± 2 ka yielded by an intercalated reworked volcaniclastic layer [Marra et al., 2016a].

### 6.1.3 Volcanic Deposits

No reliable identification for most of the volcanic deposits described in the stratigraphic logs of boreholes performed by private companies could be made, due to the lack of specific expertise on the local volcanic stratigraphy by the writers of the reports, combined with the extreme diversification and subjectivity of the adopted descriptive terminology (see next section). Indeed, boreholes that are usually performed for civil engineering purposes are aimed at assessing the mechanic characteristics of the cored rocks (e.g., coherence, texture, grainsize, etc.), independent from their correct chronostratigraphic attribution.

However, through the analysis of a selected set of outcrops and borecores directly observed by the readers or described with great detail in the literature (Fig. 12a-a′), we have verified that the primary volcanic deposits which occur in Rome are essentially those reported in Figure 12b. These are the six pyroclastic-flow deposits of the Eruption Cycles occurred at Colli Albani during the Tuscolano-Artemisio Phase, 561 through 365 ka (Tufo Pisolitico di Trigoria, Tufo del Palatino, Tufo di Acque Albule, Pozzolane Nere, Pozzolane Rosse, Tufo Lionato/Pozzolanelle) and the distal, both channel or overbank facies of three pyroclastic-flow deposits erupted by the Monti Sabatini 546 through 510 ka (Tufo Giallo della Via Tiberina, Tufo Giallo di Prima Porta, Grottarossa Pyroclastic Sequence unit b). Moreover, fallout deposits erupted by the Monti Sabatini and Vico are intercalated with the pyroclastic-flow deposits and the paleosols developed at their top. These are represented by variably thick, more or less deeply pedogenized ash-lapilli horizons, with intercalated, discontinuous pumice and scoria layers. Finally, intervening volcaniclastic deposits, deriving from reworking and re-deposition of all these volcanic products, fill the paleo-incisions excavated during periods of sea-level fall.

The lateral correlation of the selected stratigraphic data is reported in cross-section of Figure 11a. The most continuous volcanic deposit is represented by the Tufo del Palatino (TP) pyroclastic-flow deposit, which occur a progressively lower elevation from NW to the SE, paralleling the trend of the Plio-Pleistocene marine substrate in this sector (Fig. 12a′). However, while the bottom of the pyroclastic-flow deposit displays an articulated shape, consistent with its emplacement during an erosive phase, its top has sub-horizontal trend in discrete sectors, suggesting a post-depositional, tectonic dislocation.

More discontinuous is the occurrence of Tufo Pisolitico di Trigora (TPT) at the base of the volcanic succession, consistent with the marked erosive activity linked with MIS 14 sea-level fall (540 ka), responsible for its erosion. A variably thick package of reworked volcaniclastic deposits occurs between TPT and TP, representing the early MIS 13.3 aggradational succession in this area (Valle Giulia Formation). A detailed description of these volcaniclastic deposits, possibly including the primary basal fallout deposit of Tufo Giallo della Via Tibertina [Luberti et al., 2017], is reported in inset c of Figure 12.

A previously unidentified, 50 cm thick deposit of Tufo di Acque Albule (TAA) has been recognized in the present work only in one borehole drilled by the DAINST near Porta Pia [D'Ambrosio et al., 2023], confirming the occurrence of this pyroclastic flow only in the northernmost area of Rome (Karner et al., 2001a). A detailed description of TAA and of the overbank deposits of Tufo Giallo di Prima Porta (TGPP) and Grottarossa Pyroclastic Sequence (GRPS), as well as the fallout deposits of Tufi Terrosi con Pomici Bianche (TTPB) occurring in Rome is provided in inset d of Figure 12 [Luberti et al., 2017].

Notably, the TTPB represents the most diffused volcanic product outcropping below the anthropic cover in consequence of the combined effect of extensive erosion occurred since MIS 10 and the regional uplift since 250 ka [Karner et al., 2021b; Marra et al., 2016a, 2019a, b]. Indeed, large pozzolanaceous deposits erupted during late T-A

phase (Pozzolane Rosse, Pozzolane Nere and Pozzolanelle) are preserved only in the morphological heights, where they are intercalated with thick ashfall succession from Monti Sabatini and Vico.

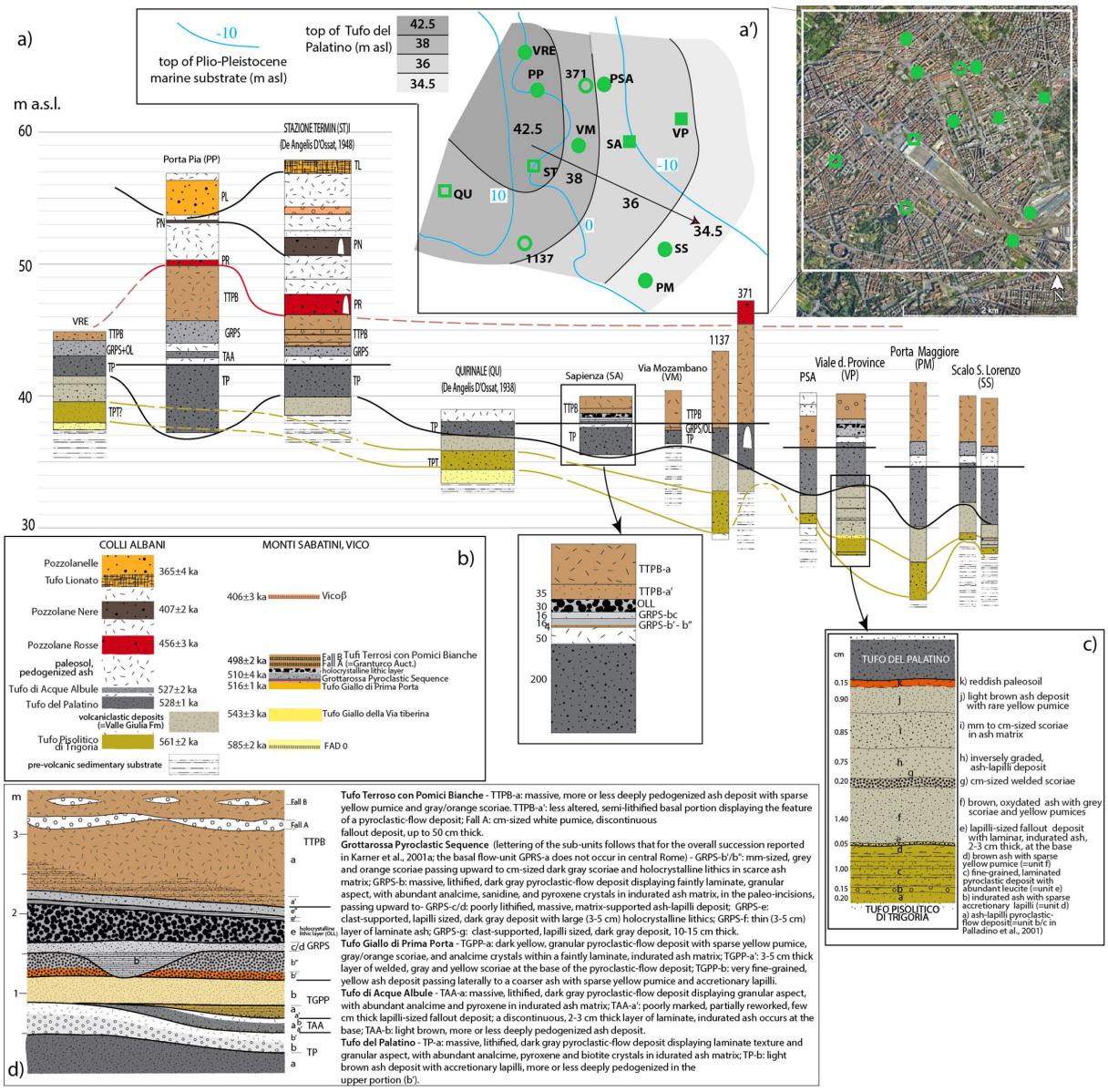


**Figure 12.** a) Attribution of the volcanic deposits to the known eruptive units (b) and lateral correlation of the observed borecores and outcrops (location in inset a′), based on the expert knowledge of their petrographic and lithologic features. c, d) Detailed description of the volcanic units [Karner et al., 2001; Luberti et al., 2017]. See text for further comments and explanation.

## 6.2 Input Parameters for the Geo-Database

Given that the primary scope of the ST-Predict project is the seismic shaking prediction of the study area, the geodatabase has been constructed using a lithologic key, taking into account that the stratigraphy of the area has solid geochronological constraints, but it is limited in area to a few dozen of sampling sites. The new boreholes drilled by the ST-Predict, and the analyses of the samples collected, have been designed to make the best use of the entire database and, in turn, to allow the entire subsurface volume to be constrained on a lithologic base.

### 6.2.1 Geo-Database Design and Implementation

In order for a dataset of paper borehole stratigraphies to be effectively codified and inserted into a databank for the 2D and 3D reconstruction of the subsurface geology for modeling purposes aimed at the study of the seismic response, it is necessary to know the limits inherent in the description and interpretation of the lithologies encountered by the boreholes, depending on the characteristics and problems linked to the local stratigraphy.

The major limitation relying into a reported stratigraphy is the subjective and often non-specialized description of the different lithologies. In the case of the Rome's stratigraphy, this is particularly true for the volcanic succession, characterized by different eruption units with different mechanisms of emplacement and lithologic/petrographic features, and for the products of their reworking which are intercalated with the primary deposits and with the fluvial-lacustrine successions (see section 5.1.3). A wide range of terms, often slang, are used in the stratigraphies for these different deposits besides the generic pozzolan and tuff (e.g., "tufo terroso", "cappellaccio", "selce", "tufite", etc.). Combined with the high degree of lateral variability, both within the same eruption unit and due to the complex pattern of unconformity limits among the different units, such problematic causes any distinction based on the stratigraphic log description devoid of reliability and inefficient for the stratigraphic reconstruction. For these reasons, we have chosen to not codify the volcanic units, with the exception of Tufo del Palatino and Tufo Lionato, which present idiosyncratic macroscopic aspect and mechanic characteristics (see section 5.1.3) and are often reliably identifiable in the log descriptions. Moreover, although not occurring in the central area of Rome, the distinction of lava-flow deposits has been provided.

Concerning the sedimentary deposits, these are represented by fining-upward aggradational successions, usually with a coarse gravel horizon at the base, several m thick, followed by a decametric package of fine-grained sediments ranging from sand to clay. Intercalations of fine gravel and carbonatic/travertine layers may occur in the sandy horizons, while diffused organic matter and peat layers characterize the clayey horizons. While the gravel is easily recognizable and always reported correctly in the logs, the fine-grained sediments are often poorly described and unified.

The "pre-volcanic" Paleotiber successions (including the aggradational successions correlated with MIS 19 to MIS 15) are easily identifiable based on the stratigraphic position with respect to the overlying volcanic succession and the underlying Pliocene marine clay substrate. In contrast, their differentiation among the different aggradational successions is impossible without specific geochronologic constraints. While this differentiation has significant implications on the reconstruction of the paleogeographic and tectonic evolution of the area and will be pursued through the forthcoming research activity, the lithological distinction between the basal gravel horizons and the overlying sandy-clay sections is sufficient for the assessment of the local seismic response.

Similarly, the attribution of the fluvial-lacustrine successions to the different aggradational successions correlated with MIS 13 to MIS 7 (Valle Giulia, San Paolo, Aurelia, and Vitinia Formations) is often hindered by the lack of chronostratigraphic markers. However, in the overall the sedimentary deposits of these successions have identical behavior with respect to the propagation of the seismic waves and will not be distinguished in the geological model.

Based on all the considerations above, the subdivision reported in Table 3 has been adopted to codify the stratigraphic logs.

The geo-DB was implemented to store the subsurface data to make it accessible not only for consultation but also as data used dynamically for three-dimensional processing and analysis. The purpose of the geo-DB is to organize a large amount of data and to present geological information in a clear, comprehensive, and efficient manner. Database development was performed within the open-source QGIS software to visualize and analyze the 2D geological data in a spatial environment. Various types of information, geometrically disaggregated, and organized into the following informational layers, georeferenced in the WGS84 UTM system, zone 33N; (i) 2D linear topographic data, including contour lines and point data (spot heights), (ii) 2D multipoint data representing boreholes, and polygonal data representing geological maps. The structure of subsurface data is essentially a relationship between a multipoint feature class (allowing for the placement of multiple points in the same position) and an associated table containing subsurface information.

The attribute tables are structured in a simple and easy-to-understand way. Each entry in the database table must be linked to the original borehole data at a specific location. This enables the three-dimensional localization of each borehole along with its geometric information in a spatial environment. Furthermore, the database can integrate files such as stratigraphic reports, geophysical data, and images like borehole log photography through

| Horizon ids | Lithofacies | Main sedimentological features |
|---|---|---|
| RI | Anthropogenic deposits (Holocene) | Heterometric and heterogeneous elements within a predominantly pyroclastic sandy-silty matrix. In some areas, they include remnants of buildings, foundation structures, walls, etc., from different epochs. At the base, these are gradually mixed or transition into the soils of the eluvial-colluvial layers of the various lithological units upon which they are overlaid. Maximum thickness 30 m. |
| AL 2 | Alluvial deposits (Holocene) | Sandy-silty and silty-clayey deposits variably interspersed with organic matter |
| AL 1 | | Coarse gravel in sand matrix |
| VU | Volcanic deposits (middle Pleistocene) | Semi-litified to incoherent scoria-flow deposits (pozzolan), lapilli-sized to ash deposits, pedogenized ash deposit (paleosoil) |
| VU-TL | Tufo Lionato | Lithified pyroclastic-flow deposit (tuff), orange in color |
| VU-TP | Tufo del Palatino | Lithified pyroclastic-flow deposit (tuff) characterized by planar lamination, dark grey in color |
| VU-LV | Lava | Lava-flow deposit |
| FL-LA 2 | Fluvial-lacustrine successions (syn-volcanic) (middle Pleistocene) | Heterogeneous sedimentary complexes, consisting of sands, sandy silts, and variously intercalated clayey silts, with abundant volcanic minerals and lenses of reworked and altered pyroclastic materials |
| FL-LA 1 | | Medium-coarse gravel (ø ≤6 cm)in sand matrix |
| PT 2 | Fluvial-lacustrine deposits (pre-volcanic) (middle-lower Pleistocene) | Silty sands and sandy-clayey silts of yellow-grey colour with calcareous concretions and local layers of travertine; Homogeneous grey clay with interspersed layers of organic matter |
| PT 1 | | Coarse gravel (ø ≤10 cm) In sand matrix |
| PL | Marine sediments (Pliocene – Early Pleistocene) | Overconsolidated clay, alternated with subordinate thinly stratified grey to yellow fine sand rich in micae. Open marine bathyal environment. |

**Table 3.** Lithofacies used to characterize the geological deposits under the city of Rome.

linking tools in QGIS. The 3D geo-DB not only provides an effective representation of interpreted objects but also allows for efficient migration to various modeling software. All data is organized in a single file, enabling exports with different formatting such as columnar, tabular, and matrices.

## 7. Conclusions

The main results of this work, aimed at providing a detailed picture of the present knowledge on the geology of Rome and describing how the newly acquired data contribute to better understand the stratigraphic setting and the geologic evolution of this area, as well as to address future development of the research, are summarized below.

– The micropaleontological analyses on samples of the marine substrate have shown the occurrence in central Rome of the two transgressive cycles previously recognized in the area to the west of the Tiber Valley. Sediments of the *G. puncticulata* biozone (Late Zanclean, 3.98-3.60 Ma) are present in the southern sector at elevation comprised between 0 and -4 m asl. Sediments characterized by the association of *G. bononiensis*, *G. crassaformis*

and *G. inflata* (MPL5b Interval subzone, ~2.6-~2.0 Ma), which is characteristic of the basal portion of the Gelasian-Calabrian ingressive cycle, occur in the center of Rome between 0 and + 20 m asl.

- The $^{40}Ar/^{39}Ar$ dating of the gravel horizon of the Monte Ciocci Formation, sampled at the type locality ~ 60 m asl, provided a maximum age of 1313 ± 3.5 ka; the lack of younger crystals strongly suggests an absolute age > 950 ka, at least, disproving previously hypothesized correlation with MIS 21. In contrast, reversed paleomagnetic polarity at VRE borecore in northern Rome allows stratigraphic and paleogeographic considerations suggesting the correlation with the oldest gravel layer occurring within the Paleotiber graben around -95 m asl, which is paleomagnetically correlated with MIS 37 (1.2 Ma).
- The age correlation between the Monte Ciocci gravel layer and the multiple gravel layers filling the Paleotiber Graben confirms the origin of such structure, which was affected by ~150 m of tectonic collapse since 1.3 Ma.
- The paleomagnetic analysis on the clay section of the aggradational succession recovered in central Rome at borehole RM-CO evidenced its normal polarity throughout, disproving previous attribution to MIS 19. Moreover, micropaleontological analysis on the clayey sediments above the basal gravel layer revealed the occurrence of two successive marine ingressions, suggesting correlation with the two consecutive isotopic peaks of MIS 15.5/15.1, consistent with the so far inferred lack of a MIS 17 aggradational succession in central Rome.
- The analysis of more than 100 stratigraphic logs of the boreholes drilled for the realization of the subway Metro C and their integration with observed cores, allowed to reconstruct an abandoned channel of the Paleotiber, between the Capitoline Hill and the Colosseum, in which the three aggradational successions correlated with MIS 15, MIS 13, and MIS 11 are embedded with each other.
- Maximum age of 551 ± 5 ka yielded by a gravel sample collected at Lapis Niger in the Roman Forum, combined with the previously unpublished dating at 548 ± 5 ka of the distal pyroclastic-flow deposit of Tufo Giallo della Via Tiberina cored at the base of the gravel layer found between -7 and -13 m asl at the Colosseum, and with the age of 534 ± 2 ka of a sample collected in the same gravel layer at ca. 9 m asl at the Capitoline Hill, allowed the attribution to MIS 13 (Valle Giulia Formation) of the aggradational succession occurring in the subsurface of the area comprised between the Capitoline Hill and the Colosseum. The marked difference in elevation characterizing the gravel layer in this sector evidences the occurrence of fault displacement affecting the subsurface of Rome.
- Such reconstruction imposes a reconsideration and partial revision of the previous chronostratigraphic setting outlined at the Palatine Hill and in the Colosseum area [e.g. Moscatelli et al., 2012; Pagliaroli et al., 2013; Mancini et al., 2014, 2023].
- The new stratigraphic, paleomagnetic, micropaleontologic and geochronologic data provided in this paper have permitted to reconstruct the geologic setting in central Rome with great detail, highlighting a coherent picture within the glacio-eustatic control on the sedimentary processes (aggradational succession model). Moreover, further detrital sanidine dating, micropaleontological and paleomagnetic analyses are in progress, which may contribute to provide insights on the control mechanism on climate change and their influence of the paleogeographic and geologic evolution of the area of Rome.
- The very complex stratigraphic framework outlined in the Historical Center of Rome, combined with the lack of visual criteria to distinguish the different aggradational successions, as well as to identify the volcanic units, imposes some limitations to the codification of the stratigraphy acquired from the borehole logs dataset, aimed at the 3D modeling. The strategy to overcome this problematic and to achieve a reliable geologic model for the assessment of the seismic response in Rome are the subject of a forthcoming, part 2 paper.

**Acknowledgments.** FM. and C.R. wish to dedicate this work to the memory of Leonardo "Leo" Lombardi, a man of great culture and extraordinary human qualities, who made a fundamental contribution to understanding the close relationship between geology and archaeology in the City of Rome, and generously shared his vast scientific knowledge. We are grateful to Superintendent Daniela Porro, Soprintendenza Speciale di Roma Archeologia, Belle Arti, Paesaggio, for authorizing the drilling of the boreholes performed within the Predict Project, to Superintendent Claudio Parisi Presicce, Sovrintendenza Capitolina ai Beni Culturali, for authorizing the sampling of the borecores stored at Musei Capitolini, and to Patrizia Fortini, Parco Archeologico del Colosseo, for allowing the sampling at *Lapis Niger*. We also thank archaeologist Mirella Serlorenzi, Soprintendenza Speciale di Roma Archeologia, Belle Arti, Paesaggio, and archaeologist Ersilia D'Ambrosio, Sovrintendenza Capitolina ai Beni Culturali, for their support.

The stratigraphic logs of the boreholes drilled along the T3 section of Line C of the Rome subway were provided by the general contractor Metro C S.c.p.a., for which we thank Ing. Eliano Romani and dott. Geol. Ivan Mammone. We would like

to thank Dott. Rita Di Giovambattista, Dott. Giuliano Milana and prof. Carlo Doglioni of INGV and Dott. Stefano Moretti and Ing. Matteo Ruggieri of IMG srl for supporting the idea and making the first meeting between the parts happen. The research activity was funded by 'Pianeta Dinamico (Dynamic Planet)-Working Earth: Geosciences For The Understanding The Dynamics Of The Earth And The Consequent Natural Risks', an INGV project funded by Ministry of University and Research through Fund for Investments of Central Administrations, Action Lines Research and innovation activities in research centers and Research and infrastructures.

## References

Alvarez, W., A.J. Ammerman, P.R. Renne, D.B. Karner, N. Terrenato and A. Montanari (1996). Quaternary fluvial-volcanic stratigraphy and geochronology of the capitoline hill in Rome, Geology, 24, 8, 751-754, https://doi.org/10.1130/0091-7613(1996)024<0751:QFVSAG>2.3.CO;2.

Barberi, F., G. Buonasorte, R. Cioni, A. Fiordelisi, L. Foresi, S. Iaccarino, M.A. Laurenzi, A. Sbrana, L. Vernia and I.M. Villa (1994). Plio-Pleistocene Geological Evolution of the Geothermal Area of Tuscany and Latium, Mem. Descr. Carta Geol. d'It., 49, 77-134.

Bellotti, P., U. Chiocchini, N. Cipriani and S. Milli (1994). I sistemi deposizionali nei sedimenti clastici pleistocenici affioranti nei dintorni di Ponte Galeria (sud ovest di Roma), Boll. Soc. Geol. Ital., 112, 924-941.

Bergamin, L., M.G. Carboni, L. Di Bella, F. Marra and I. Palagi (2000). Stratigraphical and paleoenvironmental features of the Pleistocene sediments of M. Mario (Rome), Eclogae Geol. Helvetiae, 93, 2, 265-275.

Blanc, A.C. (1939). Il giacimento musteriano di Saccopastore nel quadro del Pleistocene laziale, Riv. Antropol., 32, 1938-39, 223-235.

Boari, E., R. Avanzinelli, L. Melluso, G. Giordano, M. Mattei, A. De Benedetti, V. Morra V. and S. Conticelli (2009a). Isotope geochemistry (Sr-Nd-Pb) and petrogenesis of leucite-bearing volcanic rocks from "Colli Albani" volcano, Roman Magmatic Province, Central Italy: inferences on volcano evolution and magma genesis, Bull. Volcanol., 71, 977-1005, https://doi.org/10.1007/s00445-009-0278-6.

Bonadonna, F.P. (1968). Studi sul Pleistocene del Lazio. V. La Biostratigrafia di Monte Mario e la "Fauna Malacologica Mariana" di Cerulli-Irelli, Mem. Soc. Geol. It., 7, 261-321.

Bozzano, F., R. Funiciello, F. Marra, A. Rovelli and G. Valentini (1995). Il sottosuolo dell'area dell'Anfiteatro Flavio in Roma, Geologia Applicata e Idrogeologia, 30, Atti Convegno del Gruppo Nazionale di Geologia Applicata, 1115 giugno 1995, Giardini Naxos (ME), Italia, 417-436.

Bulian, F., A. Genesini, F. Marra, D. Scarponi and P. Vannoli (2024). New biostratigraphic and paleoecologic data on the Plio-Pleistocene paleogeographic evolution of the northeastern coastal area of the central Tyrrhenian Sea (Italy), Quat. Int., 692, 2024, 1-20, https://doi.org/10.1016/j.quaint.2024.03.011.

Caserta, A., D.M. Boore, A. Rovelli, A. Govoni, F. Marra, G. Della Monica and E. Boschi (2013). Ground motions recorded in Rome during the April 2009 L'Aquila seismic sequence: site response and comparison with ground motions from a global dataset, B. Seismol. Soc. Am., 103, 3, 2013, 1860-1874.

Cioni, R., M.A. Laurenzi, A. Sbrana and I.M. Villa (1993). $^{40}Ar/^{39}Ar$ chronostratigraphy of the initial activity in the Sabatini volcanic complex (Italy), Boll. Soc. Geol. Ital., 112, 251-263.

Conato, V., D. Esu, A. Malatesta and F. Zarlenga (1980). New data on the pleistocene of Rome, Quaternaria, 22, 131-176.

Conticelli, S., L. Francalanci, P. Manetti, R. Cioni and A. Sbrana (1997). Petrology and geochemistry of the ultrapotassic rocks from the Sabatini Volcanic District, central Italy: the role of evolutionary processes on the genesis of variably enriched alkaline magmas, J. Volcanol. Geoth. Res., 75, 107-136, https://doi.org/10.1016/S0377-0273(96)00062-5.

Corda, L., D. De Rita, F. Tecce and A. Sposato (1978). Le piroclastiti del sistema vulcanico sabatino: il complesso dei tufi stratificati varicolori de La Storta, Boll. Soc. Geol. Ital., 27, 353 and 366.

De Rita, D., R. Funiciello, U. Rossi and A. Sposato (1983). Structure and evolution of the Sacrofano-Baccano caldera, Sabatini Volcanic Complex, Rome, J. Volcanol. Geoth. Res., 17, 219-236, https://doi.org/10.1016/0377-0273(83)90069-0.

Cosentino, D., P. Cipollari, L. Di Bella, A. Esposito, C. Faranda, G. Giordano, E. Gliozzi, M. Mattei, I. Mazzini, M. Porreca and R. Funiciello (2009). Tectonics, sea- level changes and palaeoenvironments in the early Pleistocene of Rome (Italy), Quat. Res., 72, 1, 143-155, http://dx.doi.org/10.1016/j.yqres.2009.03.003.

D'Ambrosio, E., B. Giaccio, L. Lombardi, F. Marra, M.F. Rolfo and A. Sposato (2010). L'attività recente del centro eruttivo di Albano tra scienza e mito: un'analisi critica del rapporto tra il vulcano laziale e la storia dell'area albana. In Atti del VI incontro di studi "Lazio e Sabina", Roma, 2010, 125-136, Roma, Quasar.

D'Ambrosio, E., D. Diffendale, F. Marra, O. Dally, A. Danti and C. Parisi Presicce (2023). Geochemical proveniencing of the tuff used to build the Temple of Jupiter Optimus Maximus and other Archaic monuments (Rome, Italy), J. Archaeol. Sci., Reports, 51, 104146, https://doi.org/10.1016/j.jasrep.2023.104146.

De Angelis D'Ossat, G. (1938). Notizie geologiche sul Quirinale, Boll. Soc. Geol. It., 57, 174-178.

De Angelis D'Ossat, G. (1948). Osservazioni di geologia applicata sugli scavi alla Stazione Termini di Roma, Ing. Ferrov., 8, 443-50.

De Benedetti, A.A., R. Funiciello, G. Giordano, G. Diano, E. Caprilli and M. Paterne (2008). Volcanology, history and miths of the lake Albano maar (Colli Albani volcano, Italy), J. Volcanol. Geotherm. Res., 176, 387-406. http://dx.doi.org/10.1016/j.jvolgeores.2008.01.035.

De Rita, D., R. Funiciello and M. Parotto (1988). Carta geologica del complesso vulcanico dei Colli Albani (Vulcano Laziale), Progetto Final. Geodin. Consiglio Naz. delle Ric.

De Rita, D., C. Faccenna, R. Funiciello and C. Rosa (1995). Stratigraphy and Volcano-Tectonics. In: Trigila, R. (Ed.), The Volcano of the Alban Hills, Università degli Studi di Roma "La Sapienza", Rome, Italy, 33-71.

Florindo, F. and F. Marra. (1995). A revision of the stratigraphy for the middle Pleistocene continental deposits of Rome (Central Italy): Palaeomagnetic data, Ann. Geophys., 38, doi.org/10.4401/ag-4118.

Florindo, F., D.B. Karner, F. Marra, P.R. Renne, A.P. Roberts and R. Weaver (2007). Radioisotopic age constraints for glacial terminations IX and VII from aggradational sections of the Tiber River delta in Rome, Italy. Earth Planet. Sci. Lett., 256, 61-80, https://doi.org/10.1016/j.epsl.2007.01.014.

Florindo, F., F. Marra, B.R. Jicha, F. Bulian, A. Di Chiara and P. Srivastava (2024). Glacier melting triggers massive gravel deposition in central Italy's river basins, unveiling deglacial events from 1.25 to 0.78 Ma., J. Geophys. Res., Solid Earth, 129, 3, doi.org/10.1029/2023JB027877.

Fornaseri, M., A. Scherillo and U. Ventriglia (1963). La regione vulcanica dei Colli Albani, Consiglio Nazionale delle Ricerche, Roma, 561.

Freda, C., M. Gaeta, D.M. Palladino and R. Trigila (1997). The Villa Senni Eruption (Alban Hills, Central Italy): the role of H2O and CO2 on the magma chamber evolution and on the eruptive scenario, J. Volcanol. Geotherm. Res. 78, 103-120, https://doi.org/10.1016/S0377-0273(97)00007-3.

Freda, C., M. Gaeta, D.B. Karner, F. Marra, P.R. Renne, J. Taddeucci, P. Scarlato, J.N. Christensen and L. Dallai (2006). Eruptive history and petrologic evolution of the Albano multiple maar (Alban Hills, Central Italy), Bull. Volc. 68, 567-591, http://dx.doi.org/10.1007/s00445-005-0033-6.

Funiciello, R. and G. Giordano (2008a). Foglio 374 "Roma" e Note illustrative, pp. 158, Carta Geologica d'Italia, scala 1:50000eAPAT, Servizio Geologico d'Italia, Roma.

Funiciello, R. and G. Giordano (2008b). La nuova carta geologica di Roma: litostratigrafia e organizzazione stratigrafica. In: La geologia di Roma dal centro storico alla periferia, Mem. Descr. Carta Geol. D'It., 80, 39-85.

Funiciello, R. and G. Giordano (2008c). Carta geologica del Comune di Roma. Scala 1:10000. Ver.1.1 DVD. In: La geologia di Roma dal centro storico alla periferia, Mem. Descr. Carta Geol. D'It., 80.

Funiciello, R., G. Giordano and D. De Rita (2003). The Albano maar lake (Colli Albani Volcano, Italy): recent volcanic activity and evidence of pre-Roman Age catastrophic lahar events, J. Volcanol. Geotherm. Res., 123, 1, 43-61, https://doi.org/10.1016/S0377-0273(03)00027-1.

Funiciello, R., G. Giordano and M. Mattei (2008). Carta geologica del Comune di Roma. Scala 1:50000. In: La geologia di Roma dal centro storico alla periferia, Mem. Descr. Carta Geol. D'It., 80.

Gaeta, M., C. Freda, J.N. Christensen, L. Dallai, F. Marra, D.B. Karner and P. Scarlato (2006). Time-dependent geochemistry of clinopyroxene from the Alban Hills (Central Italy): Clues to the source and evolution of ultrapotassic magmas, Lithos, 86, 330-346, https://doi.org/10.1016/j.lithos.2005.05.010.

Gaeta, M., C. Freda, F. Marra, T. Di Rocco, F. Gozzi, I. Arienzo, B. Giaccio and P. Scarlato (2011). Petrology of the youngest magmas of the ultrapotassic Roman Province (Central Italy), Lithos, 127, 298-308, http://dx.doi.org/10.1016/j.lithos.2011.08.006.

Gaeta, M., C. Freda, F. Marra, I. Arienzo, F. Gozzi, B. Jicha and T. Di Rocco (2016). Paleozoic metasomatism at the origin of Mediterranean ultrapotassic magmas: constraints from time-dependent geochemistry of Colli Albani volcanic products (Central Italy), Lithos, 244, 151-164, http://dx.doi.org/10.1016/j.lithos.2015.11.034.

Giaccio, B., A. Sposato, M. Gaeta, F. Marra, D.M. Palladino, J. Taddeucci, M. Barbieri, P. Messina and M.F. Rolfo (2007). Mid-distal occurrences of the Albano Maar pyroclastic deposits and their relevance for reassessing the eruptive scenarios of the most recent activity at the Colli Albani Volcanic District, Central Italy, Quat. Int., 171, 160-178, http://dx.doi.org/10.1016/j.quaint.2006.10.013.

Giaccio, B., F. Marra, I. Hajdas, D.B. Karner, P.R. Renne and A. Sposato (2009). 40Ar/39Ar and 14C geochronology of the Albano maar deposits: implications for defining the age and eruptive style of the most recent explosive activity at the Alban Hills Volcanic District, Italy, J. Volc. Geoth. Res., 185, 203-213, http://dx.doi.org/10.1016/j.jvolgeores.2009.05.011.

Giaccio, B., G. Marino, F. Marra, L. Monaco, A. Pereira, G. Zanchetta, M. Gaeta, N. Leicher, S. Nomade, D.M. Palladino, G. Sottili, H. Guillou and V. Scao (2021). Tephrochronological constraints on the timing and nature of sea-level rise prior to and during glacial termination V, Quat. Sci. Rev., 267, https://doi.org/10.1016/j.quascirev.2021.106976.

Giordano, G., A.A. De Benedetti, A. Diana, G. Diano, F. Gaudioso, F. Marasco, M. Miceli, S. Mollo, R.A.F. Cas and R. Funiciello (2006). The Colli Albani mafic caldera (Roma, Italy): stratigraphy, structure and petrology, J. Volcanol. Geotherm. Res., 155, 49-80, http://dx.doi.org/10.1016/j.jvolgeores.2006.02.009.

Hu, H.M., G. Marino, C. Pérez-Mejías, C. Spotl, Y. Yokoyama, J. Yu, E. Rohling, A. Kano, P. Ludwig, J.G. Pinto, V. Michel, P. Valensi, X. Zhang, X. Jiang, H. Mii, W. Chien, H. Tsai, W. Sung, C. Hsu, E. Starnini, M. Zunino and C. Shen (2024). Sustained North Atlantic warming drove anomalously intense MIS 11c interglacial, Nat. Commun., 15, 5933, https://doi.org/10.1038/s41467-024-50207-1.

Jicha, B.R., B.S. Singer and P. Sobol (2016). Re-evaluation of the ages of 40Ar/39Ar sanidine standards and supereruptions in the western U.S. using a Noblesse multi-collector mass spectrometer, Chem. Geol., 431, 54-66, https://doi.org/10.1016/j.chemgeo.2016.03.024.

Karner, D.B. and F. Marra (1998). Correlation of fluviodeltaic aggradational sections with glacial climate history: a revision of the classical Pleistocene stratigraphy of Rome, Geol. Soc. Am. Bull., 110, 748-758, https://doi.org/10.1130/0016-7606(1998)110<0748:COFASW>2.3.CO;2.

Karner, D.B. and P.R. Renne (1998). 40Ar/39Ar geochronology of Roman Volcanic Province tephra in the Tiber River Valley: age calibration of middle Pleistocene sea-level changes, Geol. Soc. Am. Bull., 110, 740-747, https://doi.org/10.1130/0016-7606(1998)110<0740:AAGORV>2.3.CO;2.

Karner, D.B., F. Marra and P. Renne (2001a). The history of the Monti Sabatini and Alban Hills volcanoes: groundwork for assessing volcanic-tectonic hazards for Rome, J. Volcanol. Geoth. Res., 107, 185-219, https://doi.org/10.1016/S0377-0273(00)00258-4.

Karner, D.B., F. Marra, F. Florindo and E. Boschi (2001b). Pulsed uplift estimated from terrace elevations in the coast of Rome: evidence for a new phase of volcanic activity?, Earth Planet. Sci. Lett., 188, 135-148, https://doi.org/10.1016/S0012-821X(01)00325-9.

Karner, D.B., F. Marra and P.R. Renne (2006). Comment on: large volume phreato-magmatic ignimbrites from the Colli Albani volcano (middle pleistocene, Italy) by D. De Rita, G. Giordano, A. Esposito, M. Fabbri, and S. Rodani (JVGR (2002) 118. 77-98)., J. Volcanol. Geotherm. Res., 158, 3, 491-492, 10.1016/j.jvol-geores.2006.05.002.

Kucera, M. (2007). Chapter six planktonic foraminifera as tracers of past oceanic environments, Dev. Mar. Geol., 1, 213-262, https://doi.org/10.1016/S1572-5480(07)01011-1.

Langereis, C.G., W. Krijgsman, G. Muttoni and M. Menning (2010). Magnetostratigraphy-concepts, definitions, and applications, Newsl. Stratigr., 43, 3, 207-233, https://doi.org/10.1127/0078-0421/2010/0043-0207.

Lirer, F., L.M. Foresi, S.M. Iaccarino, G. Salvatorini, E. Turco, C. Cosentino, F.J. Sierro and A. Caruso (2019). Mediterranean Neogene planktonic foraminifer biozonation and biochronology, Earth Sci. Rev., 196, 102869, https://doi.org/10.1016/j.earscirev.2019.05.013.

Lisiecki, L.E. and M.E. Raymo (2005). A Pliocene-Pleistocene stack of 57 globally distributed benthic d18O records, Paleoceanography, 20, PA1003, http://dx.doi.org/10.1029/2004PA001071.

Luberti, G.M., F. Marra and F. Florindo (2017). A review of the stratigraphy of Rome (Italy) according to geochronologically and paleomagnetically constrained aggradational successions, glacio-eustatic forcing and volcano-tectonic processes, Quat. Int., 438, 40-67, https://doi.org/10.1016/j.quaint.2017.01.044.

Lurcock, P.C. and F. Florindo (2019). New developments in the PuffinPlot paleomagnetic data analysis program, Geochem. Geophy. Geosy., 20, 11, 5578-5587, https://doi.org/10.1029/2019GC008537.

Malinverno, A. and W.B.F. Ryan (1986). Extension in the Tyrrhenian Sea and shortening in the Apennines as results of arc migration driven by sinking of the lithosphere, Tectonics, 5, 227-245, https://doi.org/10.1029/TC005i002p00227.

Mancini, M., M. Marini, M. Moscatelli, A. Pagliaroli, F. Stigliano, C. Di Salvo, M. Simionato, G.P. Cavinato and A. Corazza (2014). A physical stratigraphy model for seismic microzonation of the Central Archaeological Area of Rome (Italy), B. Earthq. Eng., 12, 1339-1363, https://doi.org/10.1007/s10518-014-9584-2.

Mancini, M., C. Di Salvo, S. Giallini, M. Marini, M. Simionato, M.C. Cacioli, G.P. Cavinato, M. Moscatelli, F. Polpetta, P. Sirianni and F. Stigliano (2023). The subsoil of the Colosseum and the detection of the ancient Tiber River Paleovalley (MIS 12-11) in Rome, J. Mediterr. Earth Sci., 15, 10.13133/2280-6148/18067.

Marra, F. (1993). Stratigrafia e assetto geologico-strutturale dell'area romana tra il Tevere e il Rio Galeria, Geol. Romana, 29, 515-535.

Marra, F. and F. Florindo (2014). The subsurface geology of Rome: Sedimentary processes, sea-level changes and astronomical forcing, Earth Sci. Rev., 136, https://doi.org/10.1016/j.earscirev.2014.05.001.

Marra, F. and C. Rosa (1995a). Stratigrafia e assetto geologico dell'area romana, In: La geologia di Roma: il centro storico. In: Funiciello, R. (Ed.), Mem. Descr. Carta Geol. D'It, 50, 49-118.

Marra, F., M.G. Carboni, L. Di Bella, C. Faccenna, R. Funiciello and C. Rosa (1995). Il substrato plio-pleistocenico nell'Area Romana, Boll. Soc. Geol. It., 114, 195-214.

Marra, F., F. Florindo and D.B. Karner (1998). Paleomagnetism and geochronology of early Middle Pleistocene depositional sequences near Rome: comparison with the deep sea δ18O climate record, Earth Planet. Sci. Lett., 159, 147-164, https://doi.org/10.1016/S0012-821X(98)00071-5.

Marra, F., C. Freda, P. Scarlato, J. Taddeucci, D.B. Karner, P.R. Renne, M. Gaeta, D.M. Palladino, R. Trigila and G. Cavarretta (2003). Post-caldera activity in the Alban Hills Volcanic District (Italy): 40Ar/39Ar geochronology and insights into magma evolution, Bull. Volc., 65, 227-247, 10. 1007/s00445-002-0255-9.

Marra, F., F. Florindo and E. Boschi (2008). The history of glacial terminations from the Tiber River (Rome): insights to glacial forcing mechanisms, Paleoceanography, 23, PA2205. http://dx.doi.org/10.1029/2007PA001543.

Marra, F., D.B. Karner, C. Freda, M. Gaeta, D.B. Karner, P.R. Renne, M. Gaeta, D.M. Palladino, R. Trigila and G. Cavarretta (2009). Large mafic eruptions at the Alban Hills Volcanic District (Central Italy): chronostratigraphy, petrography and eruptive behavior, J. Volcanol. Geoth. Res., 179, 217 and 232, http://dx.doi.org/10.1016/j.jvolgeores.2008.11.009.

Marra, F., D. Deocampo, M.D. Jasckson and G. Ventura (2011). The Alban Hills and Monti Sabatini volcanic products used in ancient Roman masonry (Italy): an inte-grated stratigraphic, archaeological, environmental and geochemical approach, Earth Sci. Rev., 108, 115-136, http://dx.doi.org/10.1016/j.earscirev.2011.06.005.

Marra, F., F. Bozzano and F.R. Cinti (2013). Chronostratigraphic and lithologic features of the Tiber River sediments (Rome, Italy): implications on the post-glacial sea- level rise and Holocene climate, Glob. Planet. Change, 107, 157-176, http://dx.doi.org/10.1016/j.gloplacha.2013.05.002.

Marra, F., G. Sottili, M. Gaeta, B. Giaccio, B. Jicha, M. Masotta, D.M. Palladino and D. Deocampo (2014). Major explosive activity in the Sabatini Volcanic District (central Italy) over the 800-390 ka interval: geochronological-geochemical overview and tephrostratigraphic implications, Quat. Sci. Rev., 94, 74-101, http://dx.doi.org/10.1016/j.quascirev.2014.04.010.

Marra, F., P. Ceruleo, B. Jicha, L. Pandolfi, C. Petronio and L. Salari (2015a). A new age within MIS 7 for the Homo neanderthalensis of Saccopastore in the glacio- eustatically forced sedimentary successions of the Aniene River Valley, Rome, Quat. Sci. Rev., 129, 260-274, http://dx.doi.org/10.1016/j.quascirev.2015.10.027.

Marra, F., E. D'Ambrosio, M. Gaeta and M. Mattei (2015b). Petrochemical Identification and Insights on chronological employment of the volcanic aggregates used in ancient roman mortars, Archaeometry, 58, 2, 177-200, http://dx.doi.org/10.1111/arcm.12154.

Marra, F., E.J. Rohling, F. Florindo, B. Jicha, S. Nomade, A. Pereira and P.R. Renne (2016a). Independent 40Ar/39Ar and 14C age constraints on the last five glacial terminations from the aggradational successions of the Tiber River, Rome (Italy), Earth Planet Sci. Lett., 449, 105-117, http://dx.doi.org/10.1016/j.epsl.2016.05.037.

Marra, F., F. Florindo, M. Anzidei and V. Sepe (2016b). Paleo-surfaces of glacio- eustatically forced aggradational successions in the coastal area of Rome: assessing interplay between tectonics and sea-level during the last ten interglacials, Quat. Sci. Rev. 148, 85-100, http://dx.doi.org/10.1016/j.quascirev.2016.07.003.

Marra, F., B. Jicha and F. Florindo (2017). 40Ar/39Ar dating of Glacial Termination VI: constraints to the duration of Marine Isotopic Stage 13, Scientific Reports, 7, 8908, https://doi.org/10.1038/s41598-017-08614-6.

Marra, F., P. Ceruleo, L. Pandolfi, C. Petronio, M.F. Rolfo and L. Salari (2017b). The Aggradational Successions of the Aniene River Valley in Rome: Age Constraints to Early Neanderthal Presence in Europe, PLoS ONE, 12, 1, e0170434, doi:10.1371/journal.pone.0170434.

Marra, F., L. Motta, A. Brock, P. Macrì, F. Florindo, L. Sadori and N. Terrenato (2018). Rome in its setting. Post-glacial aggradation history of the Tiber River alluvial deposits and tectonic origin of the Tiber Island, Plos One, 13, 3, e0194838, https://doi.org/10.1371/journal.pone.0194838.

Marra, F., J.J. Bahain, B. Jicha, S. Nomade, D.M. Palladino, A. Pereira, C. Tolomei, P. Voinchet, M. Anzidei, D. Aureli, P. Ceruleo, C. Falguères, F. Florindo, M. Gatta, B. Ghaleb, M. La Rosa, C. Peretto, C. Petronio, R. Rocca, M. F. Rolfo, L. Salari, A. Smedile and O. Tombret (2019a). Reconstruction of the MIS 5.5, 5.3 and 5.1 coastal terraces in Latium (central Italy): a re-evaluation of the sea-level history in the Mediterranean Sea during the Last Interglacial, Quatern. Int., 525, 54-77, doi:10.1016/j.quaint.2019.09.001.

Marra, F., M. Gaeta, B.R. Jicha, C. Nicosia, C. Tolomei, P. Ceruleo, F. Florindo, M. Gatta, M. La Rosa and M.F. Rolfo (2019b). MIS 9 to MIS 5 terraces along the Tyrrhenian Sea coast of Latium (central Italy): assessing interplay between sea-level oscillations and tectonic movements, Geomorphology, 346, 10684, doi:10.1016/j.geomorph.2019.106843.

Marra, F., C. Castellano, L. Cucci, F. Florindo, M. Gaeta, B. Jicha, D.M. Palladino, G. Sottili, A. Tertulliani and C. Tolomei (2020). Monti Sabatini and Colli Albani: the dormant twin volcanoes at the gates of Rome, Sci. Rep., 10, 8666, https://doi.org/10.1038/s41598-020-65394-2.

Marra, F., A. Pereira, G. Boschian and S. Nomade (2021a). MIS 13 and MIS 11 aggradational successions of the Paleo-Tiber delta: geochronological constraints to sea-level fluctuations and to the Acheulean sites of Castel di Guido and Malagrotta (Rome, Italy), Quatern. Int., 616, 1-11, https://doi.org/10.1016/j.quaint.2021.12.016.

Marra, F., A. Brock, F. Florindo, P. Macrì, L. Motta, C. Nicosia and N. Terrenato (2021b). Faults and Fluvial Dynamism affecting the Tiber River in Prehistoric Rome, Int. Journ. Earth Science, https://doi.org/10.1007/s00531-021-02118-5.

Marra, F., A. Pereira, B. Jicha, S. Nomade, I. Biddittu, F. Florindo, G. Muttoni, E.M. Niespolo, P.R. Renne and V. Scao (2022). Terrestrial records of glacial termination V and IV and insights on deglacial mechanisms, Scientific Reports, 12:18770, https://doi.org/10.1038/s41598-022-23391-7.

Masotta, M., M. Gaeta, F. Gozzi, F. Marra, D.M. Palladino and G. Sottili (2010). $H_2O$- and temperature-zoning in magma chambers: the example of the Tufo Giallo della via Tiberina eruptions (Sabatini Volcanic District, central Italy), Lithos, 118, 119-130, https://doi.org/10.1016/j.lithos.2010.04.004.

Mattias, P.P. and U. Ventriglia (1970). La regione vulcanica dei monti Sabatini e Cimini, Mem. Soc. Geol. It., 95, 831-849.

Min, K., R. Mundil, P.R. Renne and K.R. Ludwig (2000). A test for systematic errors in $^{40}Ar/^{39}Ar$ geochronology through comparison with U/Pb analysis of a 1.1-Ga rhyolite, Geochem. Cosmochem. Acta, 64, 73-98, https://doi.org/10.1016/S0016-7037(99)00204-5.

Montone, P. and M.T. Mariucci (2016). The new release of the Italian contemporary stress map, Geophys. J. Int., 205, 3, 1525-1531, https://doi.org/10.1093/gji/ggw100.

Moscatelli, M., A. Pagliaroli, M. Mancini, F. Stigliano and G. Cavuoto (2012). Integrated subsoil model for seismic microzonation in the Central Archaeological Area of Rome (Italy), Disaster. Adv., 5, 109-124.

Opdyke, M.D. and J.E.T. Channell (1996). Magnetic stratigraphy, Academic press, 346.

Pagliaroli, A., G. Lanzo, P. Tommasi and V. Di Fiore (2013). Dynamic characterization of soils and soft rocks of the Central Archeological Area of Rome, Bull. Earthq. Eng., Special issue on Seismic Microzonation of Palatine hill, Roman Forum and Coliseum Archaeological Area, doi:10.1007/s10518-013-9452-5.

Palladino, D., M. Gaeta and F. Marra (2001). A large K-foiditic hydromagmatic eruption from the early activity of the Alban Hills Volcanic District, Italy, Bull. Volcanol., 63, 5, 345-359, https://doi.org/10.1007/s004450100150.

Parotto, M. and A. Praturlon (1975). Geological summary of the central Apennines. In: structural model of Italy. Maps and explanatory notes, Quad. Ric. Sci., 90, 257-311.

Patacca, E., R. Sartori and P. Scandone (1990). Tyrrhenian basin and apenninic arcs: Kinematic relations since late Tortonian times, Mem. Soc. Geol. Ital., 45, 425-451.

Peccerillo, A. (2017). Cenozoic Volcanism in the Tyrrhenian Sea Region, S. IAVCEI, Barcelona, Springer, 399, https://doi.org/10.1007/978-3-319-42491-0.

Pereira, A., L. Monaco, F. Marra, S. Nomade, M. Gaeta, N. Leicher, D.M. Palladino, G. Sottili, H. Guillou, V. Scao and B. Giaccio (2020). Tephrochronology of the central Mediterranean MIS 11c interglacial (~425-395 ka): New constraints from the Vico volcano and Tiber delta, central Italy, Quat. Sci. Rev., 243, 106470, https://doi.org/10.1016/j.quascirev.2020.106470.

Perini, G., L. Francalanci, J.P. Davidson and S. Conticelli (2004). Evolution and genesis of magmas from Vico volcano, Central Italy: multiple differentiation pathways and variable parental magmas, J. Petrol., 45, 139-182, https://doi.org/10.1093/petrology/egg084.

Rosa, C. (2022). La geologia e geomorfologia del versante sud ovest del Quirinale da via della Dataria al Foro di Traiano. In: Pizzo, A., Montalbano, R. (Eds.), Tra le pendici del Quirinale e il Campo Marzio. Atti delle giornate di studio dedicate a Emilio Rodríguez Almeida (Roma, 10-11 dicembre 2020), Arbor Sapientiae Editore, 55-68.

Rovelli, A., A. Caserta, L. Malagnini and F. Marra (1994). Assessment of potential strong ground motions in the city of Rome, Ann. Geofis., 37, 6, https://doi.org/10.4401/ag-4139.

Rovelli, A., L. Malagnini, A. Caserta and F. Marra (1995). Using 1-D and 2-D modelling of ground motion for seismic zonation criteria: results for the city of Rome, Ann. Geofis., 38, 5-6, 591-605, https://doi.org/10.4401/ag-4075.

Salvador, A. (1987). Unconformity bounded stratigraphic units: International Subcommission on Stratigraphic Classification (Amos Salvador, Chairman). Geol. Soc. Am. Bull., 98, 232-237, https://doi.org/10.1130/0016-7606(1987)98<232:USU>2.0.CO;2.

Scherillo, A. (1947). I Vulcani Sabatini. In: Bollettino della Società Naturalista di Napoli, 55, 125-130.

Schumm, S.A. (1993). River response to baselevel change: Implications for sequence stratigraphy, J. Geol., 101, 279-294, https://doi.org/10.1086/648221.

Serri, G., F. Innocenti and P. Manetti (1993). Geochemical and Petrological evidence of the subduction of delaminated Adriatic continental lithosphere in the genesis of the Neogene-Quaternary magmatism of Central Italy, Tectonophysics, 223, 117-147, https://doi.org/10.1016/0040-1951(93)90161-C.

Singer, B.S. (2014). A Quaternary geomagnetic instability time scale, Quat. Geochronol., 21, 29-52. doi.org/10.1016/j.quageo.2013.10.003

Sottili, G., D.M. Palladino and V. Zanon (2004). Plinian activity during the early eruptive history of the Sabatini Volcanic District, Central Italy, J. Volcanol. Geoth. Res., 135, 361-379, https://doi.org/10.1016/j.jvolgeores.2004.03.019.

Sottili, G., D.M. Palladino, F. Marra, B. Jicha, D.B. Karner and P.F. Renne (2010). Geochronology of the most recent activity in the Sabatini Volcanic District, Roman Province, central Italy, J. Volcanol. Geoth. Res., 196, 20-30, https://doi.org/10.1016/j.jvolgeores.2010.07.003.

Van der Zwaan, G., I. Duijnstee, M. Den Dulk, S. Ernst, N. Jannink and T. Kouwenhoven (1999). Benthic foraminifers: proxies or problems? A review of paleocological concepts, Earth Sci. Rev., 46, 1-4, 213-236.

Ventriglia, U. (1971). Geologia della città di Roma, Amministrazione Provinciale di Roma, 317.

Villa, I.M., I. Calanchi, E. Dinelli and F. Lucchini (1999). Age and Evolution of the Albano Crater Lake (Roman Volcanic Province), Acta Vulcanol., 11, 305-310.

*** CORRESPONDING AUTHOR: Fabrizio MARRA**

Istituto Nazionale di Geofisica e Vulcanologia, Via Vigna Murata 605, 00143, Roma, Italy

e-mail: fabrizio.marra@ingv.it